

國立交通大學

資訊科學與工程研究所

碩士論文

在廣用無線通道模型上無線網路內的孤立節點數

The Number of Isolated Nodes in Wireless Networks with
Generalized Channel Models

研究生：郭哲瑋

指導教授：易志偉 教授

中華民國九十七年十月

在廣用無線通道模型上無線網路內的孤立節點數

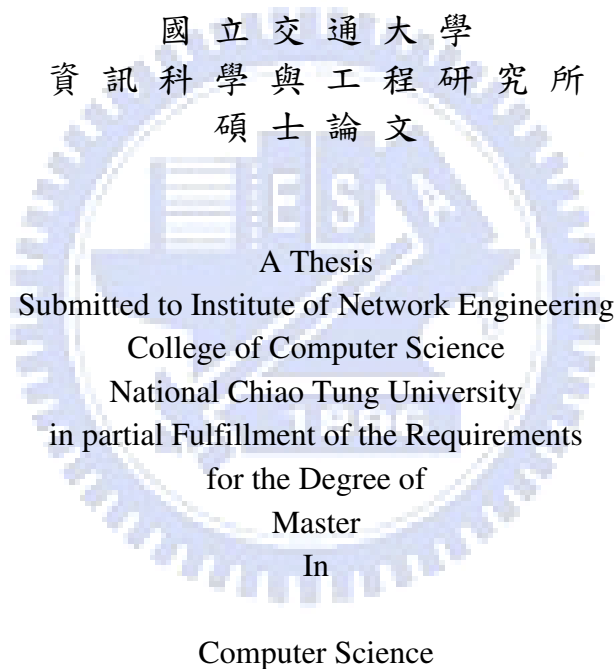
The Number of Isolated Nodes in Wireless Networks with
Generalized Channel Models

研究生：郭哲瑋

Student : Zhe-Wei Kuo

指導教授：易志偉

Advisor : Chih-Wei Yi



October 2008
Hsinchu, Taiwan, Republic of China

中華民國九十七年十月

在廣用無線通道模型上無線網路內的孤立節點數

學生：郭哲璋

指導教授：易志偉

國立交通大學

資訊科學與工程研究所

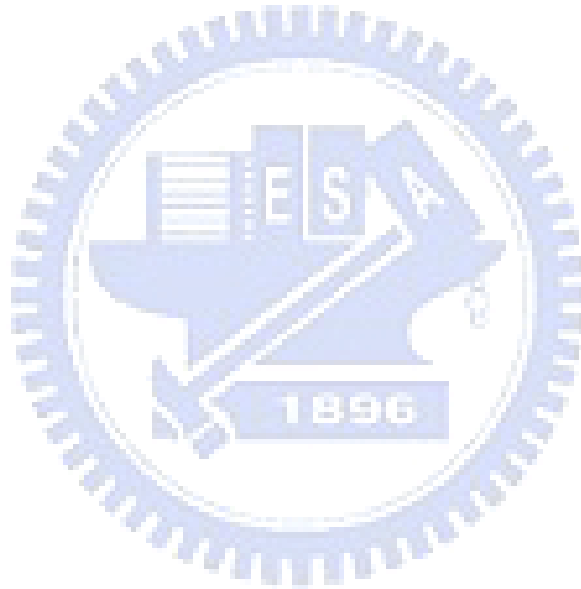
摘要

在大型無線隨意網路中，網路中孤立節點的存在與否，可視為網路連通性的指標。在現實生活中，隨著不同環境的影響和限制，我們須選取不同的網路通道模型來評估網路的可靠性和連通性。在此篇論文中，我們將藉由分析與推導來計算網路中的孤立節點數的期望值與機率分佈。

假設無線網路的節點是以平均值為 λ 的普瓦松點過程分布在邊長為 l 的正方形區域內，每個節點都具有相同的傳輸功率，且此傳輸功率是固定的，並不會隨著 l 的大小而改變。若兩個節點的相對距離為 r ，則令 $f(r)$ 代表此兩節點的連線機率。假設 $f(r)$ 是在 $[0, \infty)$ 內的遞減函數。令 $a = \int_0^{R_2} f(r) 2\pi r dr$ 且 $\lambda = \frac{1}{a}(\ln l^2 + \ln \ln l^2 + \xi)$ ，其中 ξ 是某個常數，並且令 $\omega = \xi + \ln a$ 。在此文中，我們證明在一個網路中的孤立節點個數的期望值是 $e^{-\omega}$ 。此外，隨著 $l \rightarrow \infty$ ，網路中孤立節點個數的機率分佈將會漸近於以 $e^{-\omega}$ 為平均值的普瓦松分佈。為了驗證理論的正確性，我們模擬了數個較常使用的網路通道模型，並且觀察在不同 l 大小下，對於網路要達到連通性所需的網路節點數的變化比較。

關鍵字

連通性，孤立節點，普瓦松點過程，圓盤圖，對數常態分佈，傳遞耗損模型，慢速
衰減通道，快速衰減通道，中上衰減通道



The Number of Isolated Nodes in Wireless Networks with Generalized Channel Models

Student: Zhe-Wei Kuo

Advisor: Dr. Chih-Wei Yi

National Chiao Tung University

Institute of Computer Science and Engineering

Abstract

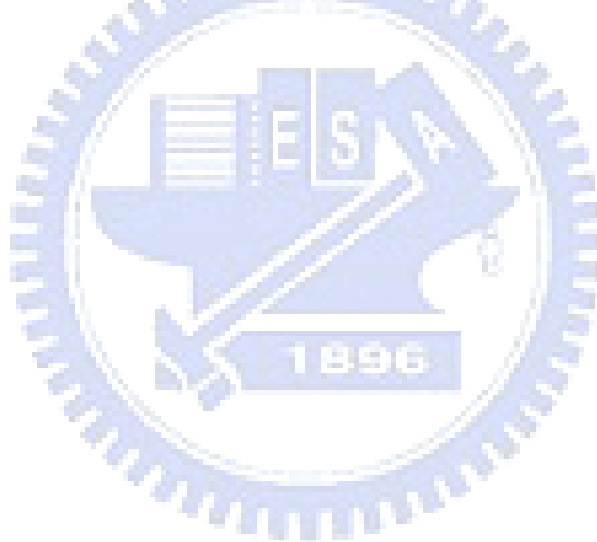
In large-scale wireless ad hoc networks the exist of isolated nodes can be used as an indicated of network connectivity. In real world, we often use different network channel models to construct networks by considering the effect and restriction of different environment. Evaluating the reliability and connectivity base on the network channel model which be chosen. In this thesis, we will analysis the expected distribution of isolated nodes in networks.

Assume wireless nodes are deployed by a Poisson point process with density λ over a deployment region $D=[0,l]^2$, and every node has the same transmission power that is fixed and will not change with l . Let $f(r)$ be the probability of the event that two nodes have a link if they are apart from each other by r . Assume $f(r)$ is a decreasing function on $[0,\infty)$ with bounded supports. Let $a = \int_0^{R_2} f(r)2\pi r dr$ and $\lambda = \frac{1}{a}(\ln l^2 + \ln \ln l^2 + \zeta)$ for some constant ζ , and let $\omega = \zeta + \ln a$. In our work, we proved that the expected number of isolated nodes in a network is $e^{-\omega}$. In addition, as

$l \rightarrow \infty$, the number of isolated nodes is asymptotically Poisson with mean $e^{-\omega}$. In order to verify our theorem, we also simulate several popular network channel models and observe the variation of the number of network's nodes in different l while considering the connectivity property.

Keywords

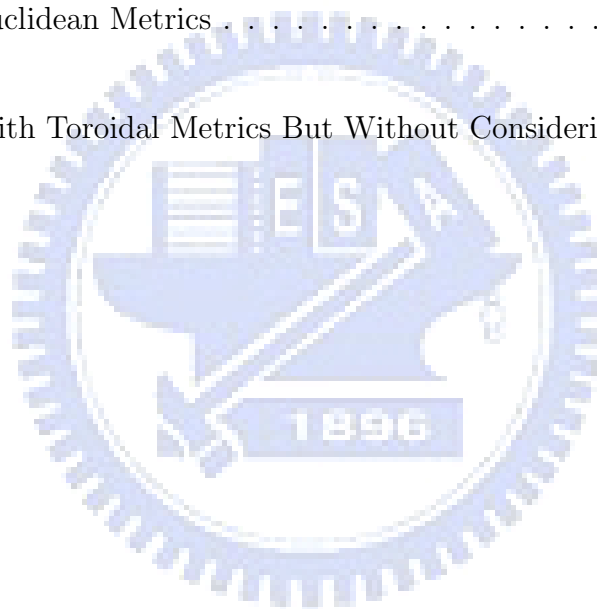
connectivity, isolated nodes, Poisson point processes, disk graphs, log-normal distribution, path-loss model, slow fading channel, fast fading channel, Nakagami fading channel.



Contents

1	Introduction	1
1.1	Wireless Ad Hoc Network	1
1.2	Research Issue and Motivation	2
1.3	Related Work	3
2	Wireless Channels	5
2.1	The Disk Model	5
2.2	The Bernoulli Model	6
2.3	The Slow Fading Model	6
2.4	The Fast Fading Model	8
2.5	The Nakagami Fading Model	10
3	The Expected Number of Isolated Nodes	14
3.1	The Expected Number	15
3.2	Proof of The Expected Number Theorem	15
3.3	Simulations	19
4	Asymptotic Distribution of the Number of Isolated Nodes	21

4.1	Probability Distribution	21
4.2	Proof of Probability Distribution Theorem	22
5	Connectivity Analysis by Simulations	31
5.1	Simulation Models and Environments	32
5.2	Examples of Network Topology	32
5.3	PDF and CDF of Connectivity	36
5.3.1	Toroidal Metrics	37
5.3.2	Euclidean Metrics	39
5.3.3	With Toroidal Metrics But Without Considering R_2	41
6	Conclusions	45



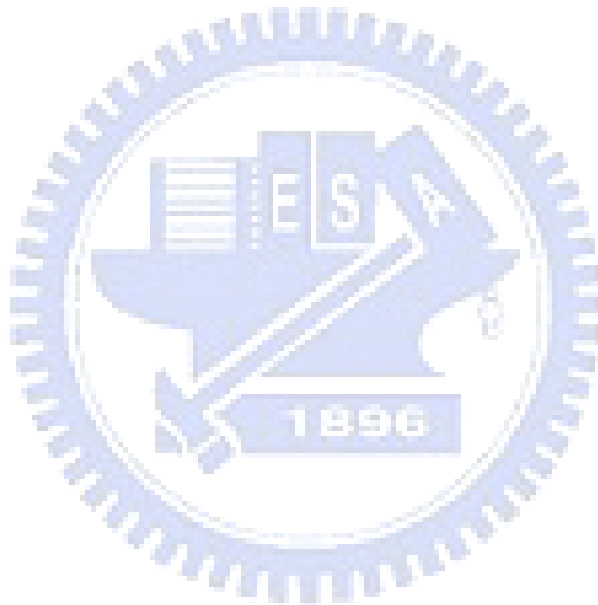
List of Figures

2.1	In a 15×15 square region, in slow fading model, nodes that have links with the centered node are shown.	7
2.2	The probability density function of slow fading model.	7
2.3	The Cumulative density function of slow fading model.	8
2.4	In a 40×40 square region, in fast fading model, nodes that have links with the centered node are shown.	9
2.5	The probability density function of fast fading model.	10
2.6	The Cumulative density function of fast fading model.	10
2.7	In a 30×30 square region, in nakagami fading model, nodes that have links with the centered node are shown.	11
2.8	The probability density function of nakagami fading model.	12
2.9	The Cumulative density function of nakagami fading model.	12
3.1	The average number of isolated nodes in networks with $l = 500$ over slow fading channel.	19
3.2	The distribution of the number of isolated nodes.	20
4.1	$\theta(\rho, r)$ is the angle of the arc of $\partial B_r(x_2)$ not contained in $B_{R_2}(x_1)$	24

4.2	A annulus with center at x_1	25
5.1	The graph of $f(r)$ in each link model.	33
5.2	In a 30×30 square region, given $R_1 = 0$ and $R_2 = 10$ in disk model, nodes that have links with the centered node are shown.	34
5.3	In a 30×30 square region, given $R_1 = 0$ and $R_2 = 11.2$ in Bernoulli model, nodes that have links with the centered node are shown.	34
5.4	In a 30×30 square region, given $R_1 = 0$ and $R_2 = 13.18597$ in slow fading model, nodes that have links with the centered node are shown.	35
5.5	In a 30×30 square region, given $R_1 = 0$ and $R_2 = 28.3$ in Nakagami fading model, nodes that have links with the centered node are shown.	36
5.6	In a 45×45 square region, given $R_1 = 0$ and $R_2 = 38.1$ in fast fading model, nodes that have links with the centered node are shown.	36
5.7	An instance of networks with $R_1 = 0$, $R_2 = 13.18597$ and $\lambda = 0.02$ in a square of $l = 100$ in slow fading model.	37
5.8	An instance of network with $R_1 = 0$, $R_2 = 10$ and $\lambda = 0.02$ in a square of $l = 100$ in disk model.	38
5.9	An instance of network with $R_1 = 0$, $R_2 = 11.2$ and $\lambda = 0.02$ in a square of $l = 100$ in Bernoulli model.	38
5.10	An instance of network with $R_1 = 0$, $R_2 = 38.1$ and $\lambda = 0.02$ in a square of $l = 100$ in fast fading model.	39
5.11	An instance of network with $R_1 = 0$, $R_2 = 23.8$ and $\lambda = 0.02$ in a square of $l = 100$ in Nakagami fading model.	39

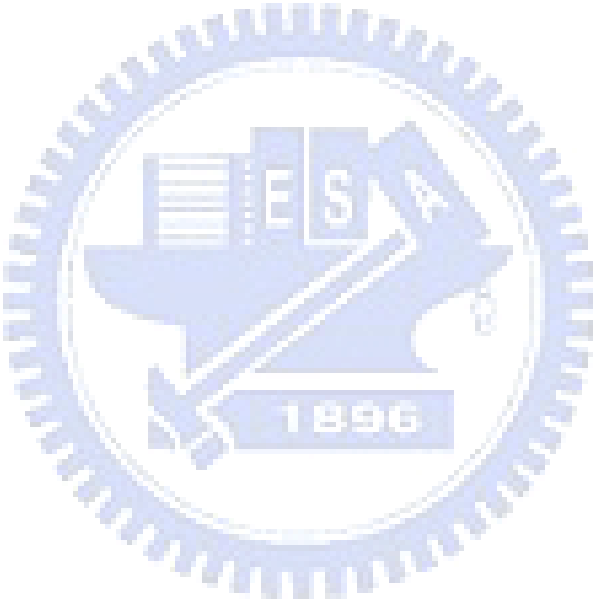
5.12	The cdfs of D_{iso} , D_{con} and D_{th} in the squares of $l = 200$, $l = 500$ and $l = 800$ in Bernoulli model with $R_1 = 0$, $R_2 = 11.2$ and $f(x) = 0.8$	40
5.13	The cdfs of D_{iso} , D_{con} and D_{th} in the squares of $l = 200$, $l = 500$ and $l = 800$ over slow fading channels with $R_1 = 0$, $R_2 = 13.18597$ and $f(r) = \frac{1}{2} \left(1 + \operatorname{erf} \left(\frac{5-5 \log r}{2\sqrt{2}} \right) \right)$	40
5.14	The cdfs of D_{iso} , D_{con} and D_{th} in the squares of $l = 200$, $l = 500$ and $l = 800$ over disk channels with $R_1 = 0$, $R_2 = 13.18597$ and $f(r) = 1$	41
5.15	The cdfs of D_{iso} , D_{con} and D_{th} in the squares of $l = 200$, $l = 500$ and $l = 800$ over fast fading channels with $R_1 = 0$, $R_2 = 38.1$ and $f(r) = \exp \left(-\frac{r^2}{100} \right)$	41
5.16	The cdfs of D_{iso} , D_{con} and D_{th} in the squares of $l = 200$, $l = 500$ and $l = 800$ over Nakagami fading channels with $R_1 = 0$, $R_2 = 23.8$ and $f(r) = \left(\frac{r^2}{50} + 1 \right) e^{-\frac{r^2}{50}}$	42
5.17	The cdfs of D_{iso} , D_{con} and D_{th} in the squares of $l = 200$ and $l = 800$ in Bernoulli model with $R_1 = 0$, $R_2 = 11.2$ and $f(x) = 0.8$ without torus.	43
5.18	The cdfs of D_{iso} , D_{con} and D_{th} in the squares of $l = 200$ and $l = 800$ in fast fading model with $R_1 = 0$, $R_2 = 38.1$ and $f(x) = \exp \left(-\frac{r^2}{100} \right)$ without torus.	43
5.19	The cdfs of D_{iso} , D_{con} and D_{th} in the squares of $l = 200$ and $l = 800$ in Disk model with $R_1 = 0$, $R_2 = 10$ and $f(x) = 1$ without torus.	43
5.20	The cdfs of D_{iso} , D_{con} and D_{th} in the squares of $l = 200$ and $l = 800$ in Slow fading model with $R_1 = 0$, $R_2 = 13.18597$ and $f(x) = \frac{1}{2} \left(1 + \operatorname{erf} \left(\frac{5-5 \log r}{2\sqrt{2}} \right) \right)$ without torus.	44

5.21 The cdfs of D_{iso} , D_{con} and D_{th} in the squares of $l = 200$ and $l = 800$ in fast fading model with $R_1 = 0$, $R_2 = 38.1$ and $f(x) = \exp\left(-\frac{x^2}{100}\right)$ without R2. 44



List of Tables

5.1 The density differences between D_{iso} and D_{con} for $p = 0.5$ 42



Chapter 1

Introduction

1.1 Wireless Ad Hoc Network

In recent years, there has been wide interest in wireless ad hoc networks. A wireless ad hoc network is a collection of wireless devices distributed in a geographic region, that forms a decentralized wireless network. 'Ad hoc' represents that each node is willing to forward data for other nodes, and so the decision on which nodes forward data is made dynamically based on the network connectivity. Each device in the network can communicate through either direct links with nearby nodes or multi-hop communication sessions with far apart nodes. Due to the lack of fixed infrastructures, wireless ad hoc networks can be flexibly deployed with low cost for various missions. Wireless ad hoc networks can be further classified by their application.

Mobile ad hoc networks : A self-configuring network of mobile routers. Nodes can move randomly and organize themselves arbitrarily. Hence, network topology may change significantly in short time period.

Wireless mesh networks : All radio nodes are static but has highly reliable and redundancy. When one node fails, the rest of network nodes can still communicate with each other. Node has self form and self heal characteristic.

Wireless sensor networks : A wireless sensor network consists of distributed autonomous sensors to acquire environment status, such as temperature, luminosity, pressure, and motion.

1.2 Research Issue and Motivation

In wireless ad hoc network, without infrastructures, connectivity, a vital property to many applications, becomes a major concern [1], [2], [3], [4]. If a network is not connected, the network will be composed of several independent components, and members belong to different components cannot exchange information with each other. This situation does not satisfying the basic function : communication of a network.

Research on the connectivity problem often focus on two issues : *the number of isolated nodes in the network* and *the connected property of a network*. Node is called isolated if it does not have a link to other nodes. Network is connected if any two nodes in the network can communicate through one or multi-hops.

Based on the requirement of connectivity, we are interested in the number of isolated nodes in a network in our work. Thus, we have theoretical derivation to estimate the number of isolated nodes in networks and also simulate several popular network models to verify our theoretical results.

1.3 Related Work

In the past, most theoretical studies of connectivity were based on a disk model in which two nodes have a link if and only if the distance between them is no more than r [5]. This model is too simple to precisely depict behaviors of networks over wireless channels. In this work, we study the connectivity of randomly-deployed wireless networks in a generalized channel model.

In many applications, such like wireless sensor networks, wireless devices are deployed in a large volume and distributed in a random manner. Therefore, it is natural to represent wireless nodes by a random point set. No existing of isolated nodes is a prerequisite of connectivity. In 1989, it was proved in [6] that if n nodes with transmission radius $\sqrt{\frac{\ln n + \xi}{\pi n}}$ for some constant ξ are independently distributed over a unit-area square, the network asymptotically has no isolated nodes with probability $\exp(-e^{-\xi})$. In 1998, it was proved in [7] that if n nodes are distributed over a unit-area disk, the network is asymptotically connected if $\xi \rightarrow \infty$ and asymptotically not connected if $\xi \rightarrow -\infty$. However, both works did not consider the possibility of node or link failures. In [8], assuming each node has the same probability p_1 to be failed and each link has the same probability p_2 to be down, authors proved that if the transmission radius is given by $\sqrt{\frac{\ln n + \xi}{\pi p_1 p_2 n}}$, the total number of isolated active nodes is asymptotically Poisson with mean $p_1 e^{-\xi}$. But in the real world, the probability of existence of a link between two nodes is highly related to the distance between them instead of a constant. In [9], [10], [11], the impact on connectivity due to link failures caused by shadowing or fading was investigated.

We will not apply a scaling model here, e.g. the one used in [7] or [8], in which the

deployment region is fixed and the transmission radius is expressed as a function of the number of nodes. Instead, we assume wireless nodes are represented by a Poisson point process with density λ over a deployment region $\mathbb{D} = [0, l]^2$. Here λ is a function of l , but for convenience, we always suppress the parameter l of λ . Every node has the same transmission power that is fixed and won't change with l . For any two nodes, let $f(r)$ be the probability of the event that these two nodes have a link if they are apart from each other by r . Without loss of generality, we assume $f(r)$ is a decreasing function on $[0, \infty)$ with bounded supports, and exists two constants $0 \leq R_1 \leq R_2 < \infty$ such that $f(r) = 1$ if $0 \leq r \leq R_1$ and $f(r) = 0$ if $r > R_2$. To avoid tedious argument about boundary effect and simplify the calculation, we apply the torus convention, for example, described in [12], [13], [14]. Hence, instead of Euclidean distance, we use toroidal distance [15], [16]. Let $d(u, v)$ denote the (toroidal) distance between nodes u and v . In addition, in what follows, let $a = \int_0^{R_2} f(r) 2\pi r dr$.

As we mentioned before, the vanishment of isolated nodes is not only a prerequisite but also a good indication for network connectivity. So ∇ , we first derive the expected number of isolated nodes. Then, we further prove that the probability distribution of the number of isolated nodes asymptotically follows Poisson distribution. The explicit formulas given in this work allow people to control the expected number of isolated nodes by tuning the node density or even transmission power. Thus, desired level of connectivity can be expected. We run extensive simulations to verify our probability analysis. As a remark, we conjecture that no isolated nodes asymptotically imply connectivity. This conjecture is also verified through simulations.

Chapter 2

Wireless Channels

Here, we introduce several link models, including disk model, Bernoulli link model, slow fading channel model, fast fading channel model and Nakagami fading channel model. We will introduce the parameters in Chapter 5.

Let α denote the path loss exponent and S_{ref} (dB) be the signal power measured at a reference distance d_0 . For convenience, we assume the reference distance $d_0 = 1$. Due to the path loss, the signal measured at a distance r apart is $S_{ref} - 10\alpha \log r$. Let S_{thr} (dB) be the minimum signal power that a signal can be decoded.

2.1 The Disk Model

In the disk model, we assume links exist whenever signals do not decay below S_{thr} . Due to the monotonic properties, let R_D denote the transmission radius. Based on log-distance path loss model in [17], we have

$$S_{thr} = S_{ref} - 10\alpha \log R_D.$$

Therefore, $R_D = 10^{\frac{S_{ref} - S_{thr}}{10\alpha}}$.

2.2 The Bernoulli Model

In a realistic environment, signal strength is not the only factor for the existence of links. To capture the uncertainty, the Bernoulli link model is a variation of disk model in which two nodes may have a link with some constant probability p if they are within the transmission range each other. So, in the Bernoulli link model, $R_1 = 0$ and $f(r) = p$. Let R_B denote the R_2 in the Bernoulli link model.

2.3 The Slow Fading Model

In the slow fading channel model [17], a signal measured at distance r apart from the transmitter is with strength $S_{ref} - 10\alpha \log r - L_{SF}$. Here L_{SF} is a log-normal random variable due to slow fading. The pdf and cdf of a normal distribution with mean μ and standard deviation σ are

$$n(x) = \frac{1}{\sigma\sqrt{2\pi}} \exp\left(-\frac{(x-\mu)^2}{2\sigma^2}\right)$$

and

$$N(x) = \frac{1}{2} \left(1 + \operatorname{erf}\left(\frac{x-\mu}{\sigma\sqrt{2}}\right)\right)$$

respectively, where

$$\operatorname{erf}(x) = \frac{2}{\sqrt{\pi}} \int_0^x e^{-t^2} dt.$$

Figure. 2.1 is a slow fading model's snapshot of distribution of links. We consider a 15×15 grid with center at the origin and assume there is a workstation on each grid

point. If a workstation has a link to the one at the origin, the grid is marked. Figure. 2.2 is the probability density function of slow fading distribution with different parameters σ and μ . The x-axis is the variable x of slow fading from 0 to 3, and the y-axis is the corresponding probability over the variation of variable x with each association σ , and $\mu = 0$. And Figure. 2.3 is the cumulative density function of slow fading.

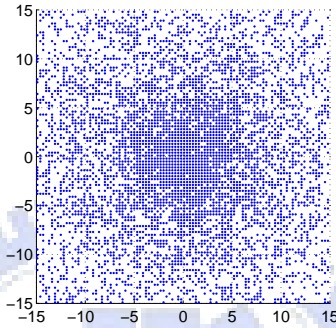


Figure 2.1: In a 15×15 square region, in slow fading model, nodes that have links with the centered node are shown.

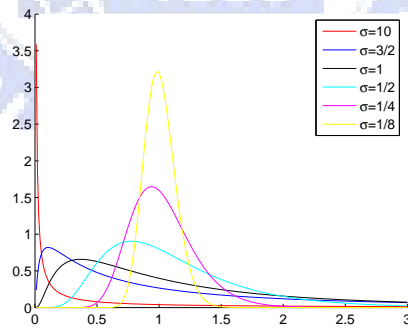


Figure 2.2: The probability density function of slow fading model.

Note that $\mu = 0$ in the slow fading model. For successful reception, the received signal

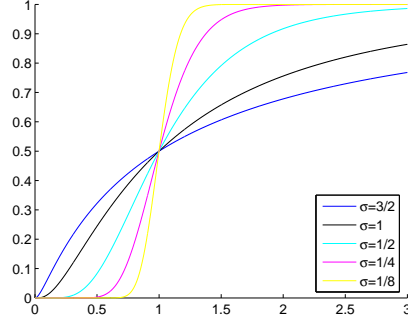


Figure 2.3: The Cumulative density function of slow fading model.

strength must be larger than S_{thr} . Therefore,

$$\begin{aligned}
 f(r) &= \Pr(L_{SF} \leq S_{ref} - S_{thr} - 10\alpha \log r) \\
 &= N(S_{ref} - S_{thr} - 10\alpha \log r) \\
 &= \frac{1}{2} \left(1 + \operatorname{erf} \left(\frac{S_{ref} - S_{thr} - 10\alpha \log r}{\sigma\sqrt{2}} \right) \right).
 \end{aligned}$$

Let R_S denote the R_2 in the slow fading model. To keep the mean node degree the same, we have

$$\pi R_D^2 = 2\pi \int_0^{R_S} \frac{1}{2} \left(1 + \operatorname{erf} \left(\frac{S_{ref} - S_{thr} - 10\alpha \log r}{\sigma\sqrt{2}} \right) \right) r dr.$$

2.4 The Fast Fading Model

The Rayleigh model is usually used to characterize the fast fading phenomenon [18]. Rayleigh model assumes the amplitude of a signal will vary according to a Rayleigh distribution. The pdf and cdf of a Rayleigh distribution with standard deviation σ are

$$r(x) = \frac{x}{\sigma^2} \exp\left(-\frac{x^2}{2\sigma^2}\right), (0 \leq x \leq \infty)$$

and

$$R(x) = 1 - \exp\left(-\frac{x^2}{2\sigma^2}\right)$$

respectively.

Figure. 2.4 is a slow fading model's snapshot of distribution of links. We consider a 40×40 grid with center at the origin and assume there is a workstation on each grid point. If a workstation has a link to the one at the origin, the grid is marked. Figure. 2.5 is the probability density function of slow fading distribution with different parameter σ . The x-axis is the variable x of slow fading from 0 to 10, and the y-axis is the corresponding probability over the variation of variable x with each σ . And Figure. 2.6 is the cumulative density function of slow fading.

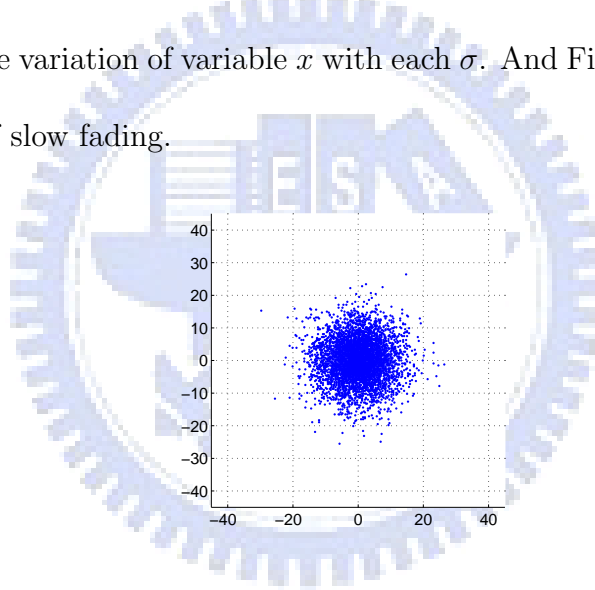


Figure 2.4: In a 40×40 square region, in fast fading model, nodes that have links with the centered node are shown.

Here $2\sigma^2$ is equal to the mean square value $E(x^2)$. After some derivation, we have $f(r) = \exp\left(-\frac{r^\alpha}{10 \frac{S_{ref} - S_{thr}}{10}}\right)$. To keep the mean node degree the same, let R_F denote the R_2 in the fast fading model and satisfy

$$\pi R_D^2 = 2\pi \int_0^{R_F} \exp\left(-\frac{r^\alpha}{10 \frac{S_{ref} - S_{thr}}{10}}\right) r dr.$$

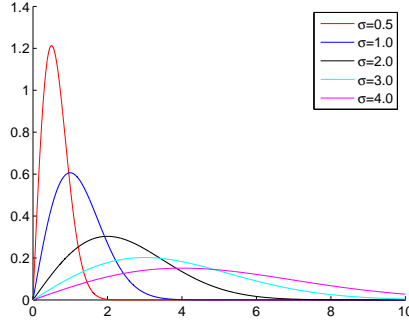


Figure 2.5: The probability density function of fast fading model.

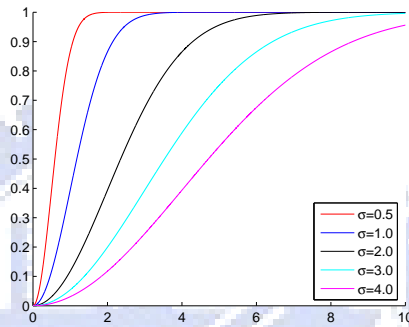


Figure 2.6: The Cumulative density function of fast fading model.

2.5 The Nakagami Fading Model

The Nakagami fading model suggests the magnitude of the received envelope obeys a Nakagami distribution. The pdf of the Nakagami distribution is

$$p(x) = 2 \left(\frac{\mu}{\omega}\right)^{\mu} \frac{1}{\Gamma(\mu)} x^{2\mu-1} e^{-\frac{\mu}{\omega}x^2},$$

where μ is the shape parameter, denoting the severity of fading, and ω is the scale parameter, equaling $E(x^2)$. In the case $\mu = 1$, the distribution reduces to a Rayleigh distribution. If x has a Nakagami distribution with parameters μ and ω , then x^2 has a gamma distribution with shape parameter μ and scale parameter $\frac{\omega}{\mu}$. The pdf and cdf of

a gamma function are

$$g(x) = x^{\mu-1} \frac{e^{-\frac{x}{\omega}}}{\left(\frac{\omega}{\mu}\right)^{\mu} \Gamma(\mu)}$$

and

$$G(x) = \frac{\gamma\left(\mu, \frac{x}{\omega}\right)}{\Gamma(\mu)}.$$

Figure. 2.7 is a slow fading model's snapshot of distribution of links. Where consider a 30×30 grid with center at the origin and assume there is a workstation on each grid point. If a workstation has a link to the one at the origin, the grid is marked. Figure. 2.8 is the probability density function of slow fading distribution with different parameters ω and μ . The x-axis is the variable x of slow fading from 0 to 3, and the y-axis is the corresponding probability over the variation of variable x with each association ω and μ . And Figure. 2.9 is the cumulative density function of slow fading.

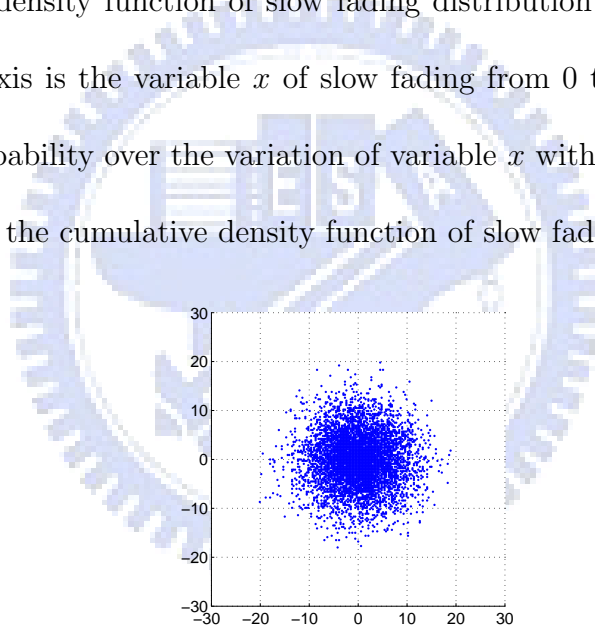


Figure 2.7: In a 30×30 square region, in nakagami fading model, nodes that have links with the centered node are shown.

The average received power at distance r is $10^{\frac{S_{ref}-10\alpha \log r}{10}}$, so $\omega = 10^{\frac{S_{ref}-10\alpha \log r}{10}}$. There-

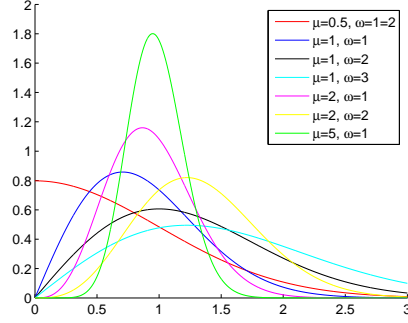


Figure 2.8: The probability density function of nakagami fading model.

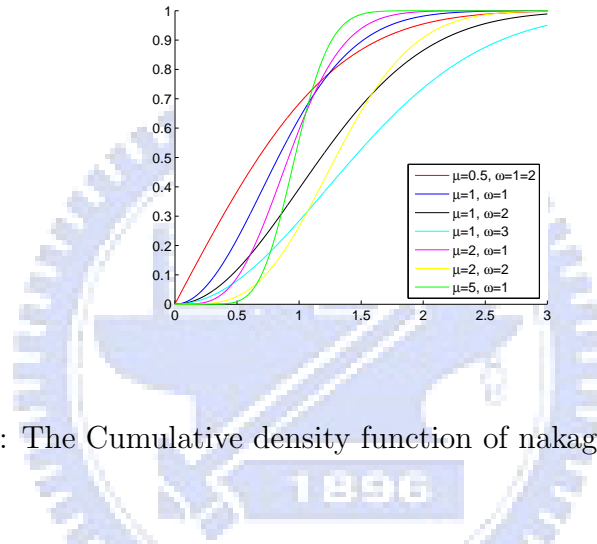


Figure 2.9: The Cumulative density function of nakagami fading model.

fore,

$$\begin{aligned}
 f(r) &= \Pr\left(x \geq 10^{\frac{S_{thr}}{10}}\right) \\
 &= 1 - G\left(10^{\frac{S_{thr}}{10}}\right) \\
 &= 1 - \frac{\gamma\left(\mu, \frac{10^{\frac{S_{thr}}{10}}}{\frac{S_{ref} - 10\alpha \log r}{10}}\right)}{\Gamma(\mu)}.
 \end{aligned}$$

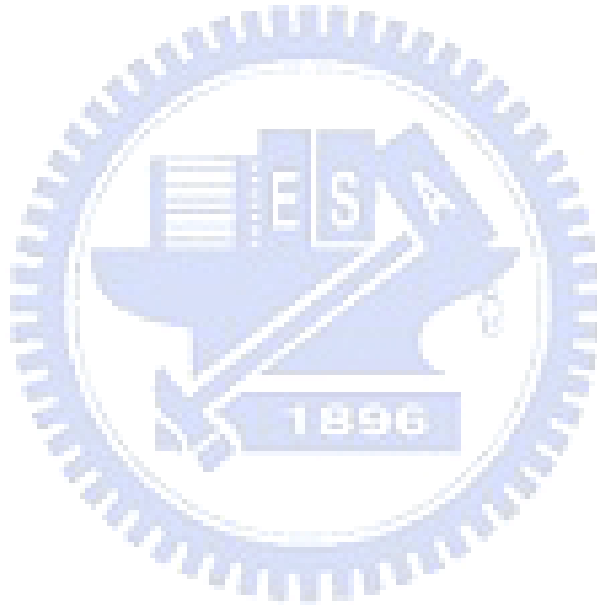
Let R_N denote the R_2 in the Nakagami distribution, then R_N satisfies

$$\pi R_D^2 = 2\pi \int_0^{R_N} \left(1 - \frac{\gamma\left(\mu, \frac{10^{\frac{S_{thr}}{10}}}{\frac{S_{ref} - 10\alpha \log r}{10}}\right)}{\Gamma(\mu)}\right) r dr.$$

$$\begin{aligned}\frac{\gamma\left(2, \frac{r^2}{50}\right)}{\Gamma(2)} &= \int_0^{\frac{r^2}{50}} te^{-t} dt \\ &= -\left(\frac{r^2}{50} + 1\right) e^{-\frac{r^2}{50}} + 1,\end{aligned}$$

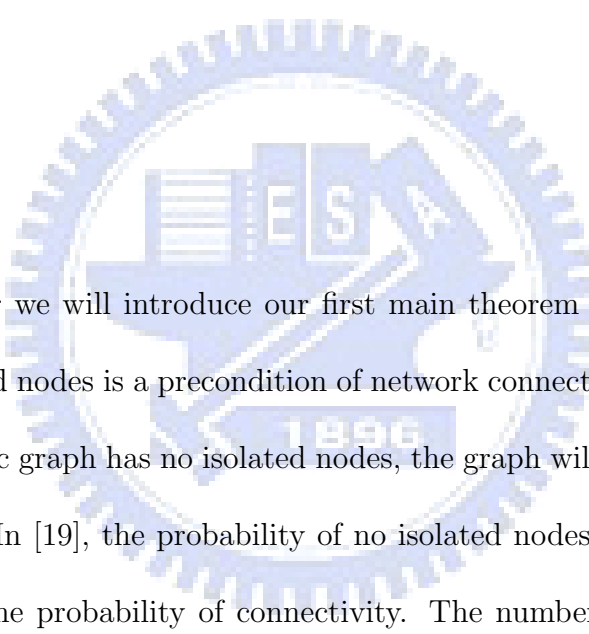
and

$$\begin{aligned}50 &= \int_0^{R_N} r \left(\frac{r^2}{50} + 1\right) e^{-\frac{r^2}{50}} dr \\ &= -\frac{1}{2} (100 + R_N^2) e^{-\frac{R_N^2}{50}} + 50.\end{aligned}$$



Chapter 3

The Expected Number of Isolated Nodes



In this Chapter we will introduce our first main theorem and its proof. The disappearance of isolated nodes is a precondition of network connectivity. It was proved that if a random geometric graph has no isolated nodes, the graph will be asymptotically almost surely connected. In [19], the probability of no isolated nodes was considered as a tight upper bound for the probability of connectivity. The number of isolated nodes can be a good index of connectivity level. To study the connectivity of wireless networks over generalized communication channels, we investigate the number of isolated nodes. The following theorem gives the expected number of isolated nodes in a network.

Remind that in what follows, $\lambda = \frac{1}{a} (\ln l^2 + \ln \ln l^2 + \xi)$ and $\omega = \xi + \ln a$.

3.1 The Expected Number

Theorem 1 *The expected number of isolated nodes is $e^{-\omega}$.*

The proof of Theorem 1 will be given in next section. Here we call $a = \int_0^{R_2} f(r) 2\pi r dr$ the *effective transmission area*, the equivalent transmission range in which signals can be clearly received. $\lambda a = \ln l^2 + \ln \ln l^2 + \xi$ can be regarded as average number of neighbors, which is the so-called *mean node degree*. According to Theorem 1, we can control the average number of isolated nodes by tuning the parameter ω that depends only on ξ and a .

Divide $\int_0^{R_2} f(r) 2\pi r dr$ by πR_2^2 . The ratio is between $\frac{R_1^2}{R_2^2}$ and 1, and is the conditional probability that two nodes have a link between them if they are within distance R_2 . If $f(r) = 1$, the ratio is equal to 1. So, any two nodes within distance R_2 always have a link, and this is the traditional random geometric graph model.

3.2 Proof of The Expected Number Theorem

In this section, we use Palm theory [20] to derive the expected number of isolated nodes. Some lemmas will be used to help the proof of theorem. For completeness, we give the Palm theory in the form used in [20].

Lemma 2 *Let $\omega = \xi + \ln a$. For any positive integer k ,*

$$\lambda^k \int_{(x_1, \dots, x_k) \in C_{kk}} e^{-k\lambda a} \left(\prod_{i=1}^k dx_i \right) \sim (e^{-\omega})^k.$$

Proof. This can be proved by straightforward calculation.

$$\begin{aligned}
& \lambda^k \int_{(x_1, \dots, x_k) \in C_{kk}} e^{-k\lambda a} \left(\prod_{i=1}^k dx_i \right) \\
&= \left(\frac{1}{a} (\ln l^2 + \ln \ln l^2 + \xi) \right)^k \left(\prod_{i=1}^k (l^2 - (i-1)\pi R_2^2) \right) e^{-k(\ln l^2 + \ln \ln l^2 + \xi)} \\
&= \left(\frac{1}{a} \right)^k e^{-k\xi} \cdot \frac{(\ln l^2 + \ln \ln l^2 + \xi)^k}{(\ln l^2)^k} \cdot \frac{\prod_{i=1}^k (l^2 - (i-1)\pi R_2^2)}{(l^2)^k} \\
&\sim \left(\frac{1}{a} e^{-\xi} \right)^k = (e^{-\omega})^k.
\end{aligned}$$

■

Theorem 3 (Palm theory) *Let \mathcal{P}_λ be a Poisson point set with mean λ . Suppose $j \in \mathbb{N}$, and suppose $h(\mathcal{Y}, \mathcal{X})$ is a bounded measurable function defined on all pairs of the form $(\mathcal{Y}, \mathcal{X})$ with \mathcal{X} a finite subset and \mathcal{Y} a subset of \mathcal{X} , satisfying $h(\mathcal{Y}, \mathcal{X}) = 0$ except when \mathcal{Y} has j elements. Then*

$$\mathbf{E} \left[\sum_{\mathcal{Y} \subseteq \mathcal{P}_\lambda} h(\mathcal{Y}, \mathcal{P}_\lambda) \right] = \frac{\lambda^j}{j!} \mathbf{E} [h(\mathcal{X}_j, \mathcal{X}_j \cup \mathcal{P}_\lambda)],$$

where the sum on the left-hand side is over all subsets \mathcal{Y} of the random Poisson point set \mathcal{P}_λ , and on the right-hand side the set \mathcal{X}_j is a binomial process with j elements, independent of \mathcal{P}_λ .

Let $\mathcal{P}_\lambda(\mathbb{D})$ denote a Poisson point process with density λ over \mathbb{D} . Let X be a random point with uniform distribution over \mathbb{D} and independent of $\mathcal{P}_\lambda(\mathbb{D})$. Let $h(\mathcal{Y}, \mathcal{X})$ for $\mathcal{Y} \subseteq \mathcal{X}$ be the indicator function such that $h(\mathcal{Y}, \mathcal{X}) = 1$ if $\#(\mathcal{Y}) = 1$ and the node in \mathcal{Y} is isolated

in \mathcal{X} ; otherwise, $h(\mathcal{Y}, \mathcal{X}) = 0$. So, we have

$$\begin{aligned}
& \text{The expected number of isolated nodes in } \mathcal{P}_\lambda(\mathbb{D}) \\
&= \sum_{\{X'\} \subseteq \mathcal{P}_\lambda(\mathbb{D})} \Pr(X' \text{ is isolated}) = \sum_{\{X'\} \subseteq \mathcal{P}_\lambda(\mathbb{D})} \mathbf{E}[h(\{X'\}, \mathcal{P}_\lambda(\mathbb{D}))] \\
&= \mathbf{E} \left[\sum_{\{X'\} \subseteq \mathcal{P}_\lambda(\mathbb{D})} h(\{X'\}, \mathcal{P}_\lambda(\mathbb{D})) \right] = (\lambda l^2) \mathbf{E}[h(\{X\}, \{X\} \cup \mathcal{P}_\lambda(\mathbb{D}))] \\
&= \lambda l^2 \Pr(X \text{ is isolated}). \tag{3.1}
\end{aligned}$$

The equality in the 3rd line is based on Palm theory, and λl^2 is the expected total number of nodes. The probability $\Pr(X \text{ is isolated})$ can be calculated by

$$\begin{aligned}
& \Pr(X \text{ is isolated}) \\
&= \int_{x \in \mathbb{D}} \Pr(X \text{ is isolated} | X = x) \Pr(X = x) dx \\
&= \frac{1}{l^2} \int_{x \in \mathbb{D}} \Pr(X \text{ is isolated} | X = x) dx. \tag{3.2}
\end{aligned}$$

To calculate $\Pr(X \text{ is isolated} | X = x)$, we apply the partition technique used in elementary calculus. The disk $B_{R_2}(x)$ is divided by k concentric circles with center at x and radii $r_1 < r_2 < \dots < r_k = R_2$ into k annuli. For convenience, let $r_0 = 0$. For $1 \leq i \leq k$, let $\Delta r_i = r_i - r_{i-1}$, and the annulus with radii r_{i-1} and r_i is called the i -th annulus. The area of the i -th annulus can be approximated by $2\pi r_i \Delta r_i$. If a node is in the i -th annulus, the event that X has a link to that node is with probability $f(r_i)$, approximately. Let N_i

denote the number of nodes in the i -th annulus. Then,

$$\begin{aligned}
& \Pr \left(\begin{array}{c} X \text{ doesn't have links with} \\ \text{nodes in the } i\text{-th annulus} \end{array} \middle| X = x \right) \\
&= \sum_{j=0}^{\infty} \Pr \left(\begin{array}{c} \text{All links between } X \text{ and} \\ \text{nodes in the } i\text{-th annulus fail} \end{array} \middle| N_i = j \right) \Pr(N_i = j | X = x) \\
&\sim \sum_{j=0}^{\infty} (1 - f(r_i))^j \left(\frac{(\lambda 2\pi r_i \Delta r_i)^j}{j!} e^{-\lambda 2\pi r_i \Delta r_i} \right) \\
&= e^{-\lambda 2\pi r_i \Delta r_i} \left(\sum_{j=0}^{\infty} (1 - f(r_i))^j \frac{(\lambda 2\pi r_i \Delta r_i)^j}{j!} \right) \\
&= e^{-\lambda 2\pi r_i \Delta r_i} e^{(1-f(r_i))\lambda 2\pi r_i \Delta r_i} = e^{-f(r_i)\lambda 2\pi r_i \Delta r_i}.
\end{aligned}$$

Therefore,

$$\begin{aligned}
& \Pr(X \text{ is isolated} | X = x) \\
&= \Pr \left(\begin{array}{c} \text{For all } 1 \leq i \leq k, \\ X \text{ doesn't have links with} \\ \text{nodes in the } i\text{-th annulus} \end{array} \middle| X = x \right) \\
&= \lim_{k \rightarrow \infty} \prod_{i=1}^k \Pr \left(\begin{array}{c} X \text{ doesn't have links with} \\ \text{nodes in the } i\text{-th annulus} \end{array} \middle| X = x \right) \\
&= \lim_{k \rightarrow \infty} \prod_{i=1}^k e^{-f(r_i)\lambda 2\pi r_i \Delta r_i} = \lim_{k \rightarrow \infty} e^{-\lambda \sum_{i=1}^k f(r_i) 2\pi r_i \Delta r_i} \\
&= e^{-\lambda \int_0^{R_2} f(r) 2\pi r dr} = e^{-\lambda a}. \tag{3.3}
\end{aligned}$$

Put (3.1), (3.2), and (3.3) together, and we have

$$\text{The expected number of isolated nodes in } \mathcal{P}_\lambda(\mathbb{D}) = \lambda \int_{x \in \mathbb{D}} e^{-\lambda a} dx \sim e^{-\omega}.$$

The last equality holds due to Lemma 2. So, Theorem 1 is proved.

3.3 Simulations

Here we shows the simulation result of first main theorem. We choose slow fading as the sample network channel model. Fig. 3.1 depicts the number of isolated nodes w.r.t. ξ in networks with $l = 500$ over slow fading channels. In Fig. 3.1, the solid line represents expected number of isolated nodes and the dotted line represents the average number of isolated nodes with simulations. The comparison between the simulation results and theoretical results verifies the accuracy of Theorems 1

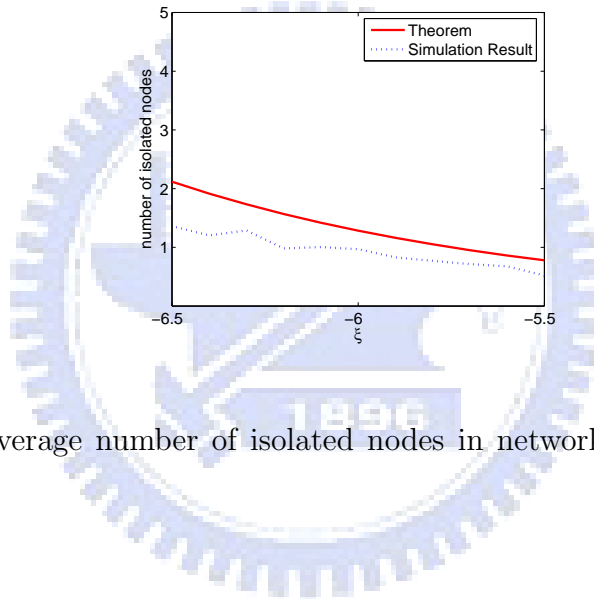


Figure 3.1: The average number of isolated nodes in networks with $l = 500$ over slow fading channel.

Next, we run another simulation. Fig. 3.2 depicts the distribution of the number of isolated nodes over slow fading channels with $\xi = -5.8$. The blue line marked with triangle is the theoretical distribution. The black line marked with star and the red line marked with circle respectively are the experimental distribution corresponding to $l = 500$ and $l = 1000$ (the corresponding densities are 0.0291 and 0.339). From this simulation, we can observe that the both the behavior of distribution of $l = 500$ and $l = 1000$ is similar to Poisson distribution. Hence, we have a conjecture that the distribution of number

of isolated nodes may approximate to the distribution of Poisson distribution, and this conjecture is proved in next chapter.

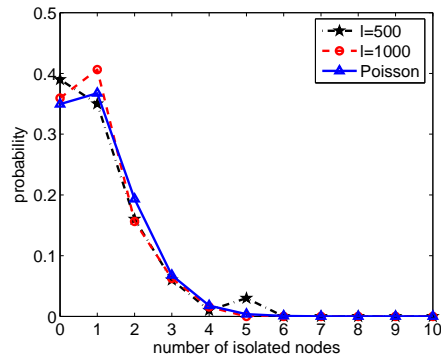
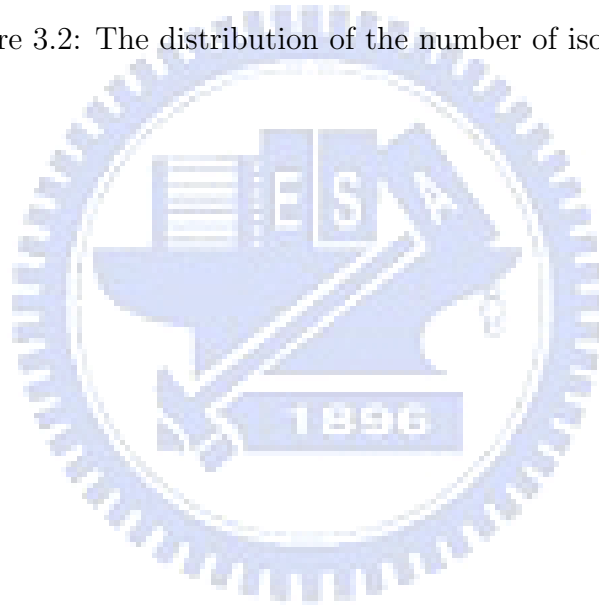


Figure 3.2: The distribution of the number of isolated nodes.



Chapter 4

Asymptotic Distribution of the Number of Isolated Nodes

In chapter 3, we have a conjecture by observing the simulation result. Thus in this chapter, we will have theoretical derivation to prove the conjecture. And more simulation results are shown in chapter 5 later.

4.1 Probability Distribution

Theorem 4 *The number of isolated nodes is asymptotically Poisson with mean $e^{-\omega}$.*

Theorem 4 will be proved in Chapter 4. According to Theorem 4, we know that a network without isolated nodes is asymptotically with probability $\exp(-e^{-\omega})$. This probability is a bound for the probability of connectivity. We conjecture that even with link failures, a network without isolated nodes is almost surely connected. If this is true, then $\Pr(\text{a network is connected}) \sim \exp(-e^{-\omega})$. This conjecture will be verified through

simulations in Chapter 5.

4.2 Proof of Probability Distribution Theorem

This section is dedicated to the proof of Theorem 4. We will apply Brun's sieve in the form, for example, used in [21] to derive the asymptotic distribution of the number of isolated nodes.

Theorem 5 (Brun's Sieve) *Assume $m(n)$ is a non-negative integer random variable.*

Let $B_1, \dots, B_{m(n)}$ be events and Y be the number of B_i that hold, and

$$S^{(j)} = \sum_{\{i_1, \dots, i_j\} \subseteq \{1, \dots, m(n)\}} \Pr(B_{i_1} \wedge \dots \wedge B_{i_j}).$$

Suppose there is a constant μ such that for every fixed j ,

$$\mathbf{E}[S^{(j)}] \sim \frac{1}{j!} \mu^j.$$

Then Y is also asymptotically Poisson with mean μ .

For convenience, let n be the total number of nodes. Let B_i for $i = 1, \dots, n$ be the event that the node X_i is isolated, and Y be the number of B_i that hold. So, Y is the total number of isolated nodes. To prove Theorem 4 by applying Brun's Sieve, we will need to show that for every fixed k ,

$$\mathbf{E} \left[\sum_{\{i_1, \dots, i_k\} \subseteq \{1, \dots, n\}} \Pr(B_{i_1} \wedge \dots \wedge B_{i_k}) \right] \sim \frac{1}{k!} (e^{-\omega})^k. \quad (4.1)$$

To apply Palm theory (Theorem 3) to prove (4.1), let $\mathcal{X}_k = \{X_1, \dots, X_k\}$ denote a uniform k -point process over \mathbb{D} and independent of $\mathcal{P}_\lambda(\mathbb{D})$, and \mathbf{B}_i for $i = 1, \dots, k$ be the

event that X_i is isolated in the network of $\mathcal{X}_k \cup \mathcal{P}_\lambda(\mathbb{D})$. Then,

$$\begin{aligned} \mathbf{E} \left[\sum_{\{i_1, \dots, i_k\} \subseteq \{1, \dots, n\}} \Pr(B_{i_1} \wedge \dots \wedge B_{i_k}) \right] &= \frac{n^k}{k!} \Pr(\mathbf{B}_1 \wedge \dots \wedge \mathbf{B}_k) \\ &= \frac{1}{k!} n^k \Pr(\mathbf{B}_1 \wedge \dots \wedge \mathbf{B}_k). \end{aligned}$$

Compared with (4.1), we can see if $n^k \Pr(\mathbf{B}_1 \wedge \dots \wedge \mathbf{B}_k) \sim (e^{-\omega})^k$, the proof is complete.

In the rest of this section, we are going to prove this.

Lemma 6 *For any integer $k \geq 2$ and $(x_1, x_2, \dots, x_k) \in C_{kk}$, we have*

$$\Pr \left(\bigwedge_{i=1}^k \mathbf{B}_i \mid \begin{array}{c} X_1 = x_1 \\ \vdots \\ X_k = x_k \end{array} \right) = e^{-k\lambda a}.$$

Proof. For any $(x_1, \dots, x_k) \in C_{kk}$, since $B_{R_2}(x_1), \dots, B_{R_2}(x_k)$ are pairwise disjoint, we have

$$\begin{aligned} \Pr \left(\bigwedge_{i=1}^k \mathbf{B}_i \mid \begin{array}{c} X_1 = x_1 \\ \vdots \\ X_k = x_k \end{array} \right) &= \prod_{i=1}^k \Pr(\mathbf{B}_i | X_i = x_i) \\ &= e^{-k\lambda a}. \end{aligned}$$

■

Lemma 7 *For any two integers $k \geq 2$ and $1 \leq m \leq k-1$, there exists a positive constant c such that for any $(x_1, \dots, x_k) \in C_{km}$,*

$$\Pr \left(\bigwedge_{i=1}^k \mathbf{B}_i \mid \begin{array}{c} X_1 = x_1 \\ \vdots \\ X_k = x_k \end{array} \right) \leq e^{-(m+c)\lambda a}.$$

Proof. First, we prove the inequality for $k = 2$ and $m = 1$. Consider the case in which $d(x_1, x_2) \geq \frac{1}{2}R_2$. Let \mathbf{B}'_2 be the event that X_2 doesn't have links to nodes in $B_{R_2}(x_2) - B_{R_2}(x_1)$. Then,

$$\Pr \left(\mathbf{B}_1 \wedge \mathbf{B}_2 \middle| \begin{array}{l} X_1 = x_1 \\ X_2 = x_2 \end{array} \right) \leq \Pr(\mathbf{B}_1 | X_1 = x_1) \Pr \left(\mathbf{B}'_2 \middle| \begin{array}{l} X_1 = x_1 \\ X_2 = x_2 \end{array} \right).$$

Since it is known from (3.3) that $\Pr(\mathbf{B}_1 | X_1 = x_1) = e^{-\lambda a}$, we only need to show that there exists a positive constant c_1 such that

$$\Pr \left(\mathbf{B}'_2 \middle| \begin{array}{l} X_1 = x_1 \\ X_2 = x_2 \end{array} \right) \leq e^{-c_1 \lambda a}.$$

Let $\rho = d(x_1, x_2)$. For any $\rho \in [\frac{1}{2}R_2, R_2]$ and $r \in [0, R_2]$, let $\theta(\rho, r)$ denote the angle of the arc of $\partial B_r(x_2)$ not contained in $B_{R_2}(x_1)$. See Fig. 4.1. Since $\theta(\rho, r)$ is increasing

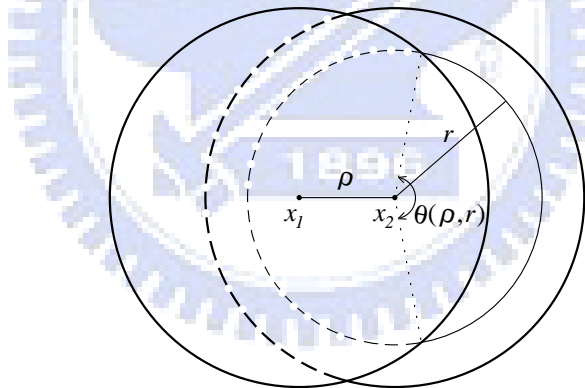


Figure 4.1: $\theta(\rho, r)$ is the angle of the arc of $\partial B_r(x_2)$ not contained in $B_{R_2}(x_1)$.

w.r.t. ρ and $f(r) \geq 0$ for $r \in [0, R_2]$, we have

$$\int_0^{R_2} f(r) \theta(\rho, r) r dr \geq \int_{\frac{1}{2}R_2}^{R_2} f(r) \theta\left(\frac{1}{2}R_2, r\right) r dr,$$

and let

$$c_1 = \frac{\int_{\frac{1}{2}R_2}^{R_2} f(r) \theta\left(\frac{1}{2}R_2, r\right) r dr}{\int_0^{R_2} f(r) \theta(\rho, r) r dr}.$$

Applying the same approach in deriving the probability $\Pr(X \text{ is isolated} | X = x)$ in Chapter 3, we have

$$\begin{aligned} \Pr \left(\mathbf{B}'_2 \middle| \begin{array}{l} X_1 = x_1 \\ X_2 = x_2 \end{array} \right) &= e^{-\lambda \int_0^{R_2} f(r) \theta(\rho, r) r dr} \\ &\leq e^{-\lambda \int_{\frac{1}{2}R_2}^{R_2} f(r) \theta(\frac{1}{2}R_2, r) r dr} = e^{-c_1 \lambda \int_0^{R_2} f(r) 2\pi r dr} \\ &= e^{-c_1 \lambda a}. \end{aligned}$$

Therefore, if $\frac{1}{2}R_2 \leq d(x_1, x_2) \leq R_2$, we have $\Pr \left(\mathbf{B}_1 \wedge \mathbf{B}_2 \middle| \begin{array}{l} X_1 = x_1 \\ X_2 = x_2 \end{array} \right) \leq e^{-(1+c_1)\lambda a}$.

Now, consider the case in which $0 \leq d(x_1, x_2) \leq \frac{1}{2}R_2$. For this case, we only consider nodes in $B_{R_2}(x_1)$ and divide $B_{R_2}(x_1)$ by h concentric circles with center at x_1 and radii $r_1 < r_2 < \dots < r_h = R_2$ as illustrated in Fig. 4.2. Since $f(r)$ is a decreasing function, we

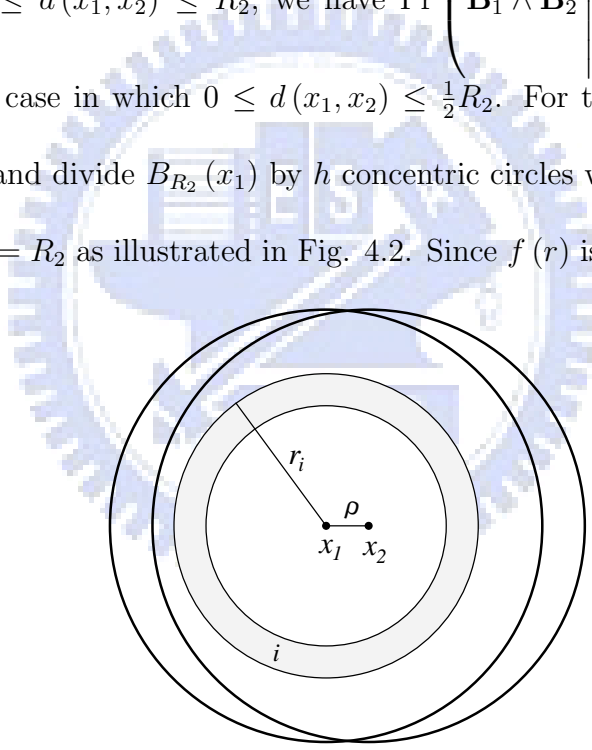


Figure 4.2: A annulus with center at x_1 .

have

$$\begin{aligned}
& \Pr \left(\begin{array}{l} X_1 \text{ and } X_2 \text{ doesn't have links} \\ \text{with nodes in the } i\text{-th annulus} \end{array} \middle| \begin{array}{l} X_1 = x_1 \\ X_2 = x_2 \end{array} \right) \\
& \leq \sum_{j=0}^{\infty} \left(\frac{(\lambda 2\pi r_i \Delta r_i)^j}{j!} e^{-\lambda 2\pi r_i \Delta r_i} \right) (1 - f(r_i))^j (1 - f(r_i + \rho))^j \\
& = e^{-(f(r_i) + f(r_i + \rho) - f(r_i)f(r_i + \rho))\lambda 2\pi r_i \Delta r_i}.
\end{aligned}$$

Note that the inequality still holds for annuli not fully contained in $B_{R_2}(x_2)$. So,

$$\begin{aligned}
& \Pr \left(\mathbf{B}_1 \wedge \mathbf{B}_2 \middle| \begin{array}{l} X_1 = x_1 \\ X_2 = x_2 \end{array} \right) \leq \lim_{k \rightarrow \infty} \prod_{i=1}^k e^{-(f(r_i) + f(r_i + \rho) - f(r_i)f(r_i + \rho))\lambda 2\pi r_i \Delta r_i} \\
& = e^{-\lambda \int_0^{R_2} (f(r) + f(r + \rho) - f(r)f(r + \rho)) 2\pi r dr} = e^{-\lambda \int_0^{R_2} f(r) 2\pi r dr - \lambda \int_0^{R_2} (f(r + \rho) - f(r)f(r + \rho)) 2\pi r dr}.
\end{aligned}$$

Since $\int_0^{R_2} f(r) 2\pi r dr = a$, if we can prove that there exists a positive constant c_2 such that $\int_0^{R_2} (f(r + \rho) - f(r)f(r + \rho)) 2\pi r dr \geq c_2 a$, then this case is also proved. For any $r \in [\frac{1}{8}R_2, \frac{1}{4}R_2]$, we have $f(r + \rho) \geq f(\frac{3}{4}R_2)$ and $1 - f(r) \geq 1 - f(\frac{1}{8}R_2)$. Let

$$c_2 = \frac{\int_{\frac{1}{8}R_2}^{\frac{1}{4}R_2} f(\frac{3}{4}R_2) (1 - f(\frac{1}{8}R_2)) 2\pi r dr}{\int_0^{R_2} f(r) 2\pi r dr}.$$

Then,

$$\begin{aligned}
& \int_0^{R_2} f(r + \rho) (1 - f(r)) 2\pi r dr \geq \int_{\frac{1}{8}R_2}^{\frac{1}{4}R_2} f(r + \rho) (1 - f(r)) 2\pi r dr \\
& \geq \int_{\frac{1}{8}R_2}^{\frac{1}{4}R_2} f\left(\frac{3}{4}R_2\right) \left(1 - f\left(\frac{1}{8}R_2\right)\right) 2\pi r dr = c_2 a.
\end{aligned}$$

So, if $0 \leq d(x_1, x_2) \leq \frac{1}{2}R_2$, we have $\Pr \left(\mathbf{B}_1 \wedge \mathbf{B}_2 \middle| \begin{array}{l} X_1 = x_1 \\ X_2 = x_2 \end{array} \right) \leq e^{-(1+c_2)\lambda a}$. Choose $c = \min(c_1, c_2)$, and the lemma for $k = 2$ is proved. For any $k \geq 3$ and $m = 1$, since

there always exist two overlapping disks in the component $\bigcup_{i=1, \dots, k} B_{R_2}(x_i)$, it is not hard to see that the inequality is still correct. For any $k \geq 3$ and $2 \leq m \leq k - 1$, if $(x_1, \dots, x_k) \in C_{km}$, then $\{x_1, \dots, x_k\}$ is partitioned into m sets K_1, K_2, \dots, K_m such that for each $j = 1, \dots, m$, $\bigcup_{x \in K_j} B_{R_2}(x)$ is a maximal component. Let $n_j = |K_j|$ be the number of elements in K_j . Suppose $K_j = \{x_{j1}, \dots, x_{jn_j}\}$. Then,

$$\Pr \left(\bigwedge_{x_i \in K_j} \mathbf{B}_i \mid \begin{array}{c} X_{j1} = x_{j1} \\ \vdots \\ X_{jn_j} = x_{jn_j} \end{array} \right) = e^{-\lambda a} \text{ if } n_j = 1; \text{ and}$$

$$\Pr \left(\bigwedge_{x_i \in K_j} \mathbf{B}_i \mid \begin{array}{c} X_{j1} = x_{j1} \\ \vdots \\ X_{jn_j} = x_{jn_j} \end{array} \right) \leq e^{-(1+c)\lambda a} \text{ if } n_j > 1.$$

Since there exists at least one component contains more than one node, we have

$$\Pr \left(\bigwedge_{i=1}^k \mathbf{B}_i \mid \begin{array}{c} X_1 = x_1 \\ \vdots \\ X_k = x_k \end{array} \right) = \prod_{j=1}^m \Pr \left(\bigwedge_{x_i \in K_j} \mathbf{B}_i \mid \begin{array}{c} X_{j1} = x_{j1} \\ \vdots \\ X_{jn_j} = x_{jn_j} \end{array} \right) \leq e^{-(m+c)\lambda a}.$$

So, the lemma is proved. ■

Lemma 8 For any two integers $k \geq 2$ and $1 \leq m \leq k - 1$,

$$\lambda^k \int_{(x_1, x_2, \dots, x_k) \in C_{km}} e^{-(m+c)\lambda a} \left(\prod_{i=1}^k dx_i \right) = o(1).$$

Proof. First, consider $m = 1$. This can be validated by straightforward calculation.

$$\begin{aligned}
& \lambda^k \int_{(x_1, x_2, \dots, x_k) \in C_{k1}} e^{-(1+c)\lambda a} \left(\prod_{i=1}^k dx_i \right) \\
& \leq \lambda^k l^2 \left(\prod_{i=2}^k (\pi (2(i-1)R_2)^2) \right) e^{-(1+c)\lambda a} \\
& = O(1) (\ln l^2 + \ln \ln l^2 + \xi)^k l^2 e^{-(1+c)(\ln l^2 + \ln \ln l^2 + \xi)} \\
& = o(1).
\end{aligned}$$

Next, we consider $2 \leq m \leq k-1$. If $(x_1, \dots, x_k) \in C_{km}$, and then $\{x_1, \dots, x_k\}$ can be partitioned into m sets K_1, K_2, \dots, K_m such that for each $j = 1, \dots, m$, $\bigcup_{x \in K_j} B_{R_2}(x)$ is a maximal connected component. Let $n_j = |K_j|$ be the number of elements in K_j , and suppose $K_j = \{x_{j1}, \dots, x_{jn_j}\}$. For fixed k and m , the number of m -partition of $\{x_1, \dots, x_k\}$ are constant. Then,

$$\begin{aligned}
& \lambda^k \int_{(x_1, x_2, \dots, x_k) \in C_{km}} e^{-(m+c)\lambda a} \left(\prod_{i=1}^k dx_i \right) \\
& = O(1) e^{-c\lambda a} \prod_{j=1}^m \left(\lambda^{n_j} \int_{(x_{j1}, \dots, x_{jn_j}) \in C_{n_j1}} e^{-\lambda a} \left(\prod_{j=1}^{n_j} dx_i \right) \right) \\
& = o(1).
\end{aligned}$$

Because the the last equality is one $n_j > 1$ at least. So, the lemma is proved. ■

Lemma 9 For any integer $k \geq 2$, $(\lambda l^2)^k \Pr(\mathbf{B}_1 \wedge \dots \wedge \mathbf{B}_k) \sim (e^{-\omega})^k$.

Proof. Let $G_r(x_1, \dots, x_k)$ denote the r -disk graph over x_1, \dots, x_k in which there is an edge between two nodes if and only if their distance is at most r . For any positive integers k and m with $1 \leq m \leq k$, let C_{km} denote the set of $(x_1, \dots, x_k) \in \mathbb{D}^k$ satisfy that $G_{2R_2}(x_1, \dots, x_k)$ has exactly m connected components. We partition \mathbb{D}^k into

$C_{k1}, C_{k2}, \dots, C_{kk}$.

$$\begin{aligned}
& (\lambda l^2)^k \Pr(\mathbf{B}_1 \wedge \dots \wedge \mathbf{B}_k) \\
&= (\lambda l^2)^k \int_{(x_1, x_2, \dots, x_k) \in \mathbb{D}^k} \Pr \left(\bigwedge_{i=1}^k \mathbf{B}_i \mid \begin{array}{c} X_1 = x_1 \\ \vdots \\ X_k = x_k \end{array} \right) \Pr \left(\begin{array}{c} X_1 = x_1 \\ \vdots \\ X_k = x_k \end{array} \right) \left(\prod_{i=1}^k dx_i \right) \\
&= \lambda^k \int_{(x_1, x_2, \dots, x_k) \in \mathbb{D}^k} \Pr \left(\bigwedge_{i=1}^k \mathbf{B}_i \mid \begin{array}{c} X_1 = x_1 \\ \vdots \\ X_k = x_k \end{array} \right) \left(\prod_{i=1}^k dx_i \right) \\
&= \sum_{i=1}^k \lambda^k \int_{(x_1, x_2, \dots, x_k) \in C_{ki}} \Pr \left(\bigwedge_{i=1}^k \mathbf{B}_i \mid \begin{array}{c} X_1 = x_1 \\ \vdots \\ X_k = x_k \end{array} \right) \left(\prod_{i=1}^k dx_i \right). \tag{4.2}
\end{aligned}$$

For the integral over C_{km} with $1 \leq m \leq k-1$, according to Lemmas 7 and 8, we have

$$\begin{aligned}
& \lambda^k \int_{(x_1, x_2, \dots, x_k) \in C_{km}} \Pr \left(\bigwedge_{i=1}^k \mathbf{B}_i \mid \begin{array}{c} X_1 = x_1 \\ \vdots \\ X_k = x_k \end{array} \right) \left(\prod_{i=1}^k dx_i \right) \\
&\leq \lambda^k \int_{(x_1, x_2, \dots, x_k) \in C_{km}} e^{-(m+c)\lambda a} \left(\prod_{i=1}^k dx_i \right) = o(1). \tag{4.3}
\end{aligned}$$

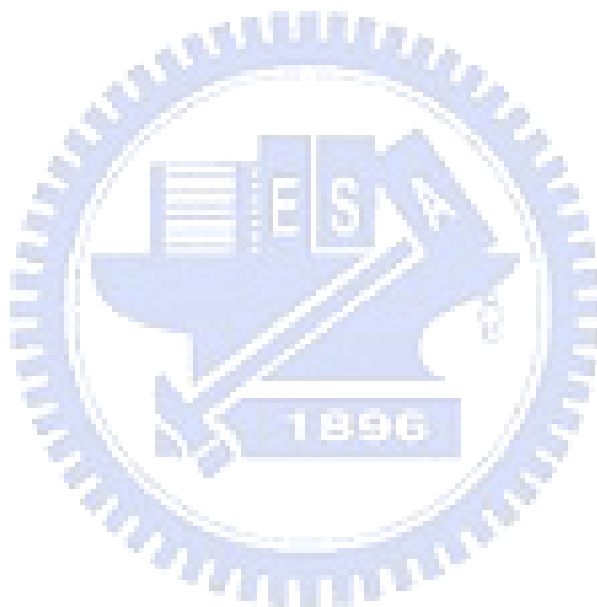
For the integral over C_{kk} , according to Lemmas 6 and 2, we have

$$\begin{aligned}
& \lambda^k \int_{(x_1, x_2, \dots, x_k) \in C_{kk}} \Pr \left(\bigwedge_{i=1}^k \mathbf{B}_i \mid \begin{array}{c} X_1 = x_1 \\ \vdots \\ X_k = x_k \end{array} \right) \left(\prod_{i=1}^k dx_i \right) \\
&= \lambda^k \int_{(x_1, x_2, \dots, x_k) \in C_{kk}} e^{-k\lambda a} \left(\prod_{i=1}^k dx_i \right) \sim (e^{-\omega})^k. \tag{4.4}
\end{aligned}$$

After putting (4.2), (4.3), and (4.4) together, and then we have

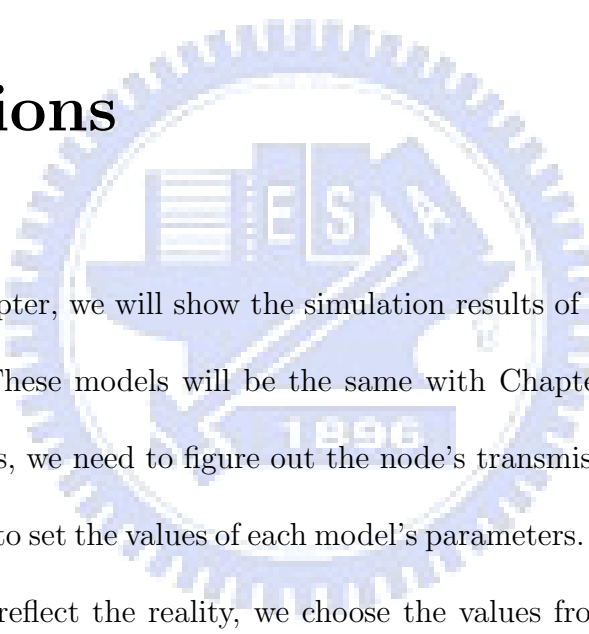
$$(\lambda l^2)^k \Pr(\mathbf{B}_1 \wedge \cdots \wedge \mathbf{B}_k) \sim (e^{-\omega})^k .$$

■



Chapter 5

Connectivity Analysis by Simulations



In this chapter, we will show the simulation results of network models that mentioned previous. These models will be the same with Chapter 2. In order to simulate the network models, we need to figure out the node's transmission radius of each model. Thus, we will need to set the values of each model's parameters. According to each model's characteristic and reflect the reality, we choose the values from each model's suggested range by their author. And without loss of generality and fairness, we assume that each node has the same transmission power and expect each node to have the same number of network neighbors.

Section 5.1 involves each network models' parameters we used in our simulations. In Section 5.2, several snapshots will be shown as samples of network topology. And in Section 5.3, we will use charts of probability distribution to discuss about the connectivity issue.

5.1 Simulation Models and Environments

Based on the condition of each node has the same number of network neighbors. We select suitable parameter's value and then we can derive to obtain the node's transmission radius in different link models. Thus, we consider transmission radius R_1 and R_2 here. If the distance between any two nodes is smaller than R_1 , they will be directly connected. If the distance between any two nodes is more than R_1 but smaller than R_2 , there will be a probability to be connected or disconnected which is determined by each models' property. If the distance between any two nodes is more than R_2 , they will be disconnected. So, in this chapter, while simulating in the disk model, we let $f(r) = 1$ and assume $\alpha = 2$, $S_{ref} = 35$ dBm, and $S_{thr} = 15$ dBm, and then we can obtain $R_1 = R_2 = 10$. To have a fair comparison in the simulation, the mean node degree in each model should be the same as that in the naive disk model. In the Bernoulli model let $p = 0.8$, so $R_1 = 0$ and $R_2 = 11.2$. In the slow fading model, we set $\sigma = 8$ dB. Therefore, $f(r) = \frac{1}{2} \left(1 + \operatorname{erf} \left(\frac{5-5\log r}{2\sqrt{2}} \right) \right)$, $R_1 = 0$, and $R_2 = 13.18597$. In the fast fading model, we set $f(r) = \exp \left(-\frac{r^2}{100} \right)$, $R_1 = 0$, and $R_2 = 38.1$. And in the Nakagami fading model, we set $\mu = 2$ in our simulation, $f(r) = 1 - \frac{\gamma}{\Gamma(2)} \frac{r^2}{50} = \left(\frac{r^2}{50} + 1 \right) e^{-\frac{r^2}{50}}$, $R_1 = 0$, and $R_2 = 28.3$.

5.2 Examples of Network Topology

In this section, we would like to give some snapshots of network topology, and our simulation will be considered the effect of toroidal metrics in this section, where toroidal metrics is a concept that the network nodes nearby the boundary of network deployment region will still have communication probability with opposite nodes which are also nearby

the boundary of network deployment region. Then we regard two opposite boundary as the same one. If two opposite nodes are inside the transmission radius with each other, then they will have probability to direct communication which is determined by the network link model.

As defined earlier, $f(r)$ is the probability of the event that two nodes have a link if they are apart from each other by r . Fig. 5.1 depicts $f(r)$ in each link model introduced in Chapter 2.

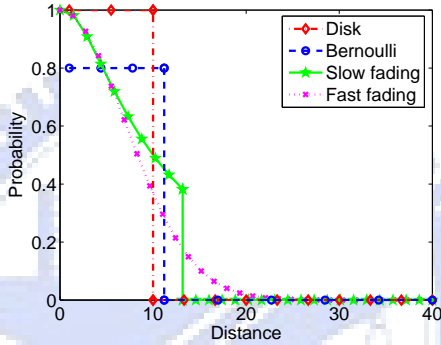


Figure 5.1: The graph of $f(r)$ in each link model.

Next, we would like to give some snapshot of our models. Unlike the snapshots we show in the chapter 2, we consider transmission radius R_1 and R_2 in this chapter. We consider a grid with center at the origin. Assume there is a workstation on each grid point. Fig. 5.2 is a disk model's snapshot of distribution of links with $R_1 = 10$, $R_2 = 10$ and $f(x) = 1$. If a workstation has a link to the one at the origin, the grid is marked.

Fig. 5.3 is a Bernoulli model's snapshot of distribution of links with $R_1 = 0$, $R_2 = 11.2$ and $f(x) = 0.8$. Because of the characteristic of Bernoulli model, each grid node inside radius R_2 will has the same probability to has a connection with the original node. The effective communication areas are uniform spread inside the transmission radius R_2 of

original node.

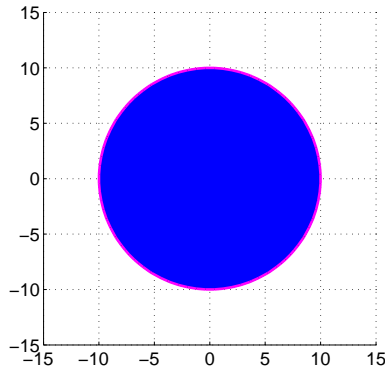


Figure 5.2: In a 30×30 square region, given $R_1 = 0$ and $R_2 = 10$ in disk model, nodes that have links with the centered node are shown.

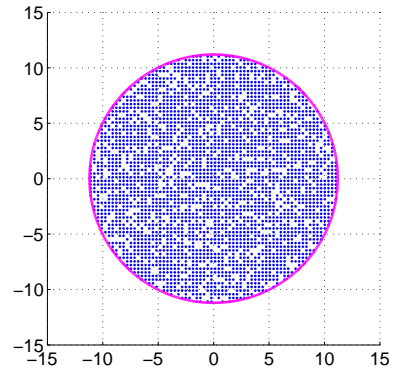


Figure 5.3: In a 30×30 square region, given $R_1 = 0$ and $R_2 = 11.2$ in Bernoulli model, nodes that have links with the centered node are shown.

Fig. 5.4 is a slow fading model's snapshot of distribution of links with $R_1 = 0$, $R_2 = 13.18597$ and $f(r) = \frac{1}{2} \left(1 + \operatorname{erf} \left(\frac{5-5 \log r}{2\sqrt{2}} \right) \right)$. We can observe that the grid nodes are closed to the original node have higher probability to communication directly, Even the grid nodes are far away from the original node still not have very low probability to communicate with original node if they still inside the R_2 of original node.

Fig. 5.5 is a snapshot of Nakagami fading model with $R_1 = 0$, $R_2 = 23.8$ and $f(r) = \left(\frac{r^2}{50} + 1 \right) e^{-\frac{r^2}{50}}$. From the snapshot, we could obtain that marked area is highly the aggregation in the nearby region of original node. In other words, in the Nakagami fading model, if the grid nodes are closed to the original node, it will have highly probability to have connection with original node. However, if the grid nodes are far away from the original nodes, they will have low probability to become an effectively communication

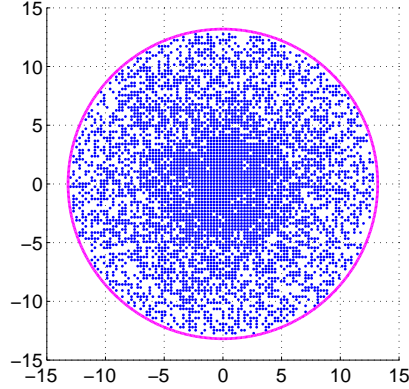


Figure 5.4: In a 30×30 square region, given $R_1 = 0$ and $R_2 = 13.18597$ in slow fading model, nodes that have links with the centered node are shown.

area. There is a little difference to slow fading model.

Fig. 5.6 is a snapshot of fast fading model $R_1 = 0$, $R_2 = 38.1$ and $f(r) = \exp\left(-\frac{r^2}{100}\right)$. From the figure, we can observe the effectively communication areas are also aggregated around the original node in the fast fading model.

Next, we would like to show the network connection state of each link model in a small deployment region.

Fig. 5.7 is an instance of wireless networks with $R_1 = 0$, $R_2 = 13.18597$ and $\lambda = 0.02$ in a square of $l = 100$ over slow fading channels. The solid line between two nodes represents that it exists a link between these two nodes. And the dotted line denotes there is a link between nodes in opposite sides due to the toroidal metric. Fig. 5.8 is an instance with $R_1 = 0$, $R_2 = 10$ and $\lambda = 0.02$ in a square of $l = 100$ over disk channels. Fig. 5.9 is an instance with $R_1 = 0$, $R_2 = 11.2$ and $\lambda = 0.02$ in a square of $l = 100$ over Bernoulli channels. Fig. 5.10 is an instance with $R_1 = 0$, $R_2 = 38.1$ and $\lambda = 0.02$ in a square of $l = 100$ over fast fading channels. Fig.5.11 is an instance with $R_1 = 0$,

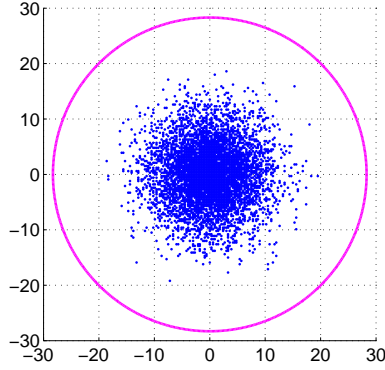


Figure 5.5: In a 30×30 square region, given $R_1 = 0$ and $R_2 = 28.3$ in Nakagami fading model, nodes that have links with the centered node are shown.

$R_2 = 23.8$ and $\lambda = 0.02$ in a square of $l = 100$ over Nakagami fading channels.

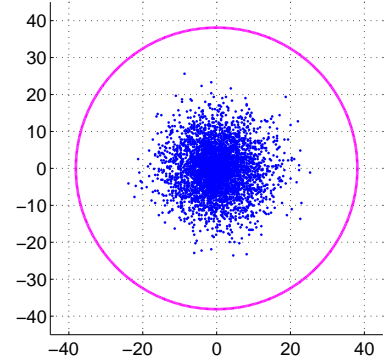


Figure 5.6: In a 45×45 square region, given $R_1 = 0$ and $R_2 = 38.1$ in fast fading model, nodes that have links with the centered node are shown.

5.3 PDF and CDF of Connectivity

In this section, we will show the simulation results of probability distribution that compares with the theoretical results on connectivity issue. We will show simulations of network channel models with considering the toroidal metrics property and without the toroidal metrics property. And we will also simulate the network channel models with considering R_2 .

For its convenience, let random variable D_{iso} be the node density for a network without isolated nodes, random variable D_{com} be the node density for a network being connected and random variable D_{th} be the theoretical node density leading to a connected network.

We use Poisson point process to generate nodes into the deployment region until there

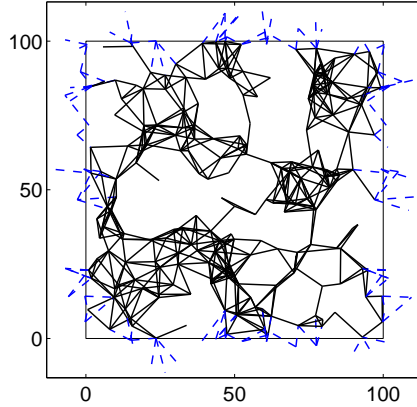


Figure 5.7: An instance of networks with $R_1 = 0$, $R_2 = 13.18597$ and $\lambda = 0.02$ in a square of $l = 100$ in slow fading model.

are no isolated nodes in the network to get D_{iso} for 400 iterations. In a similar way, we can get D_{con} .

5.3.1 Toroidal Metrics

First, we simulate network channel models with toroidal metrics property.

Fig. 5.12 shows, in Bernoulli model, with $R_1 = 0$, $R_2 = 11.2$ and $f(x) = 0.8$, the cdfs of D_{iso} , D_{con} and D_{th} in the squares of $l = 200$, $l = 500$ and $l = 800$ respectively. The results in slow fading model with $R_1 = 0$, $R_2 = 13.18597$ and $f(r) = \frac{1}{2} \left(1 + \operatorname{erf} \left(\frac{5-5 \log r}{2\sqrt{2}} \right) \right)$, are shown in Fig. 5.13, for $l = 200$, $l = 500$ and $l = 800$. Fig.5.14 shows disk model with $R_1 = 0$, $R_2 = 10$ and $f(r) = 1$, for $l = 200$, $l = 500$ and $l = 800$.

Fig.5.15 shows fast fading model with $R_1 = 0$, $R_2 = 38.1$ and $f(r) = \exp \left(-\frac{r^2}{100} \right)$, for $l = 200$, $l = 500$ and $l = 800$.

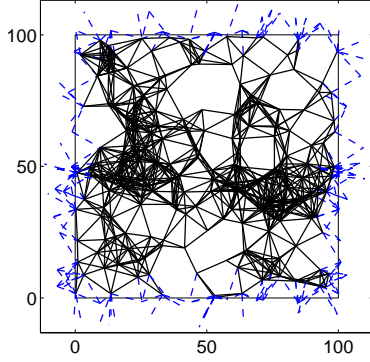


Figure 5.8: An instance of network with $R_1 = 0$, $R_2 = 10$ and $\lambda = 0.02$ in a square of $l = 100$ in disk model.

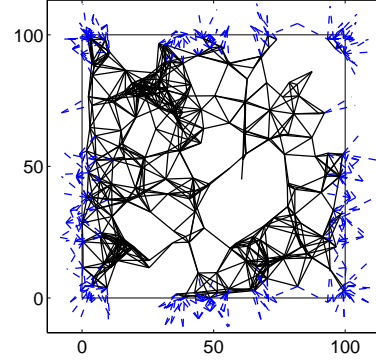


Figure 5.9: An instance of network with $R_1 = 0$, $R_2 = 11.2$ and $\lambda = 0.02$ in a square of $l = 100$ in Bernoulli model.

Fig.5.16 shows Nakagami fading model with $R_1 = 0$, $R_2 = 23.8$ and $f(r) = \left(\frac{r^2}{50} + 1\right) e^{-\frac{r^2}{50}}$, for $l = 200$, $l = 500$ and $l = 800$.

In disk, Nakagami fading and fast fading models, the cdfs resemble those in Bernoulli and slow fading models. Therefore, we can have the insight from these figures that the higher the value of l is, the closer the cdfs of D_{iso} , D_{con} and D_{th} are. These results also verify our theoretical analysis.

For grasping the convergence of graphs, Table 5.1 lists the differences between D_{iso} and D_{con} for $p = 0.5$ as $l = 200$, $l = 500$ and $l = 800$. It can be observed that the gap decreases as l increases. We can expect that $\Pr(\text{a network without isolated nodes}) \sim \Pr(\text{a network is connected})$ as $l \rightarrow \infty$. This verifies our conjecture in Chapter 3.

5.3.2 Euclidean Metrics

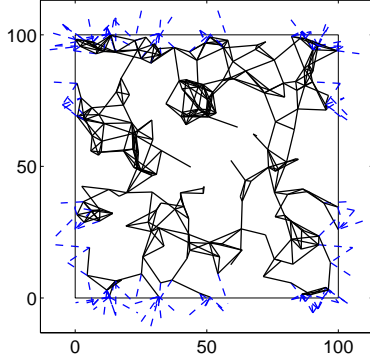


Figure 5.10: An instance of network with $R_1 = 0$, $R_2 = 38.1$ and $\lambda = 0.02$ in a square of $l = 100$ in fast fading model.

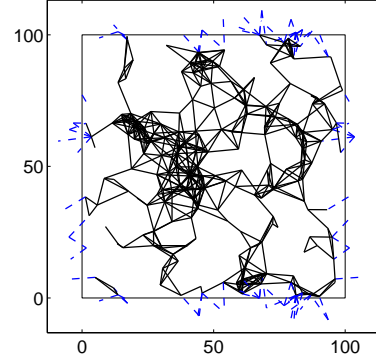


Figure 5.11: An instance of network with $R_1 = 0$, $R_2 = 23.8$ and $\lambda = 0.02$ in a square of $l = 100$ in Nakagami fading model.

In our simulations, we also simulate our each channel models without toroidal metrics property. Fig. 5.17 shows, in Bernoulli model, with $R_1 = 0$, $R_2 = 11.2$ and $f(x) = 0.8$, the cdfs of D_{iso} , D_{con} and D_{th} in the squares of $l = 200$ and $l = 800$ respectively. Fig. 5.18 shows the fast fading model, with $R_1 = 0$, $R_2 = 38.1$ and $f(r) = \exp\left(-\frac{r^2}{100}\right)$, for $l = 200$ and $l = 800$.

Generally speaking, without considering the toroidal metrics means that network need to be deployed more nodes to achieve network's connectivity. This intuition reflects on the simulations. From these simulations, we can observe that the *c.d.f.* on the models without toroidal metrics is right shift to the *c.d.f.* on the models with toroidal metrics. Also, we can observe that the behavior of 'not isolated' and 'connected' is closer to each adapter with the growth of network scale. This indicate torus constrain may lead to need to be deployed more nodes when we discuss network connectivity, but it doesn't

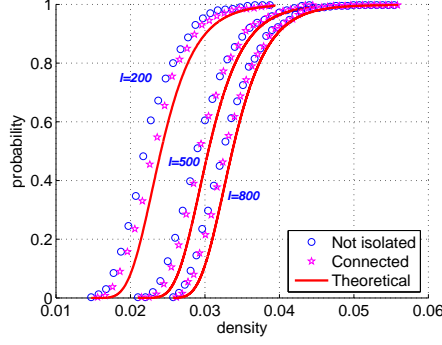


Figure 5.12: The cdfs of D_{iso} , D_{con} and D_{th} in the squares of $l = 200$, $l = 500$ and $l = 800$ in Bernoulli model with $R_1 = 0$, $R_2 = 11.2$ and $f(x) = 0.8$.

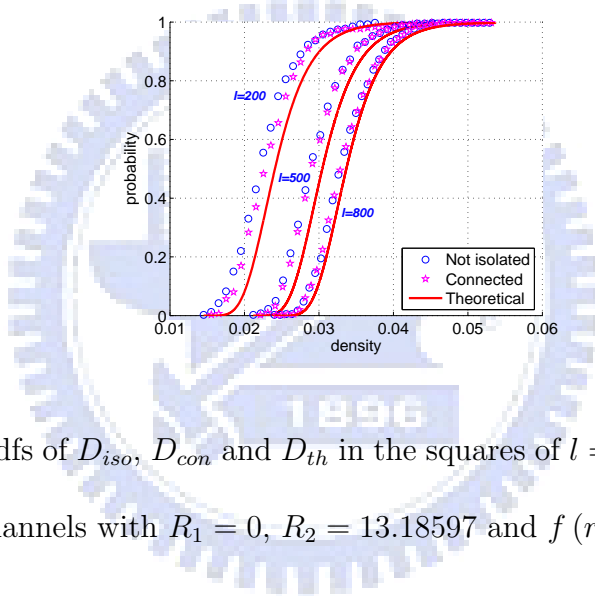


Figure 5.13: The cdfs of D_{iso} , D_{con} and D_{th} in the squares of $l = 200$, $l = 500$ and $l = 800$ over slow fading channels with $R_1 = 0$, $R_2 = 13.18597$ and $f(r) = \frac{1}{2} \left(1 + \operatorname{erf} \left(\frac{5-5 \log r}{2\sqrt{2}} \right) \right)$.

effect the convergence relationship of 'not isolated' and 'connected' while network scale is growth. Fig. 5.19 shows the disk model, with $R_1 = 0$, $R_2 = 10$ and $f(r) = 1$, for $l = 200$ and $l = 800$. Fig.5.20 shows the slow fading model, with $R_1 = 0$, $R_2 = 13.18597$ and $f(r) = \frac{1}{2} \left(1 + \operatorname{erf} \left(\frac{5-5 \log r}{2\sqrt{2}} \right) \right)$, for $l = 200$ and $l = 800$.The convergent property in both models also holds.

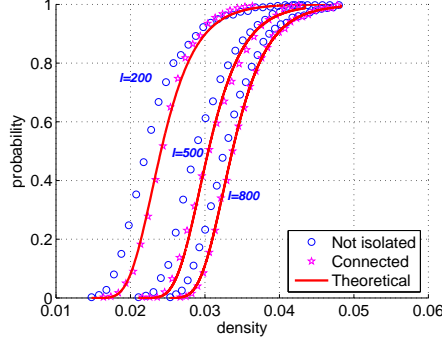


Figure 5.14: The cdfs of D_{iso} , D_{con} and D_{th} in the squares of $l = 200$, $l = 500$ and $l = 800$ over disk channels with $R_1 = 0$, $R_2 = 13.18597$ and $f(r) = 1$.

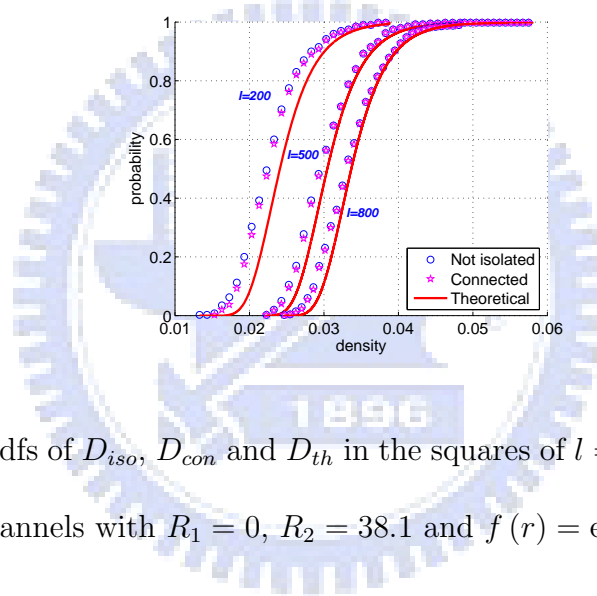


Figure 5.15: The cdfs of D_{iso} , D_{con} and D_{th} in the squares of $l = 200$, $l = 500$ and $l = 800$ over fast fading channels with $R_1 = 0$, $R_2 = 38.1$ and $f(r) = \exp\left(-\frac{r^2}{100}\right)$.

5.3.3 With Toroidal Metrics But Without Considering R_2

In the above simulations, we give bounded transmission radius R_2 in each models and force communication probability to zero while two nodes' distance exceeds R_2 . However, in the fast fading channel model and slow fading channel model, the radio signal strength decays with distance, therefore. There may be weakly radio signal while two nodes are far away more than R_2 . Next we simulate model without consider R_2 . Fig. 5.21 shows the fast fading model, with $R_1 = 0$, $R_2 = 38.1$ and $f(r) = \exp\left(-\frac{r^2}{100}\right)$, for

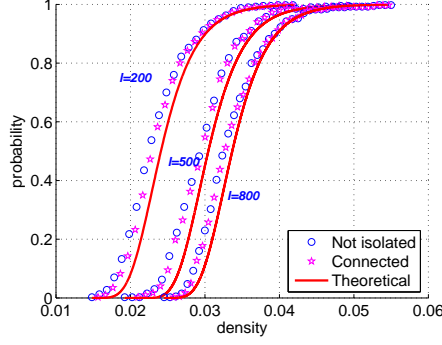


Figure 5.16: The cdfs of D_{iso} , D_{con} and D_{th} in the squares of $l = 200$, $l = 500$ and $l = 800$ over Nakagami fading channels with $R_1 = 0$, $R_2 = 23.8$ and $f(r) = \left(\frac{r^2}{50} + 1\right) e^{-\frac{r^2}{50}}$.

Table 5.1: The density differences between D_{iso} and D_{con} for $p = 0.5$.

	$l = 200$	$l = 500$	$l = 800$
Disk model	0.0022	0.00170	0.001100
Bernoulli model	0.0013	0.00038	0.000338
Slow fading model	0.0006	0.00011	0.000016
Fast fading model	0.0002	0.00013	0.000038

$l = 200$, $l = 500$ and $l = 800$ without consider R_2 . Compared with the above simulation results, we can observe that removing R_2 constraint doesn't cause drastic change on the number of deploy nodes. Although it still has weakly signal strength while two nodes' distance exceeds R_2 , the signal strength is not strong enough to support two nodes' communication.

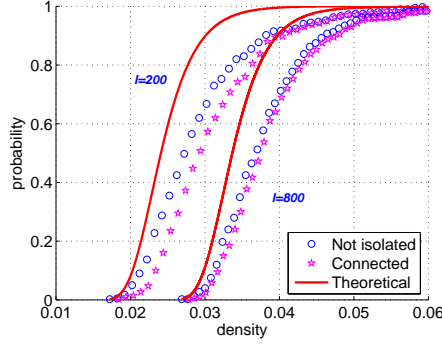


Figure 5.17: The cdfs of D_{iso} , D_{con} and D_{th} in the squares of $l = 200$ and $l = 800$ in Bernoulli model with $R_1 = 0$, $R_2 = 11.2$ and $f(x) = 0.8$ without torus.

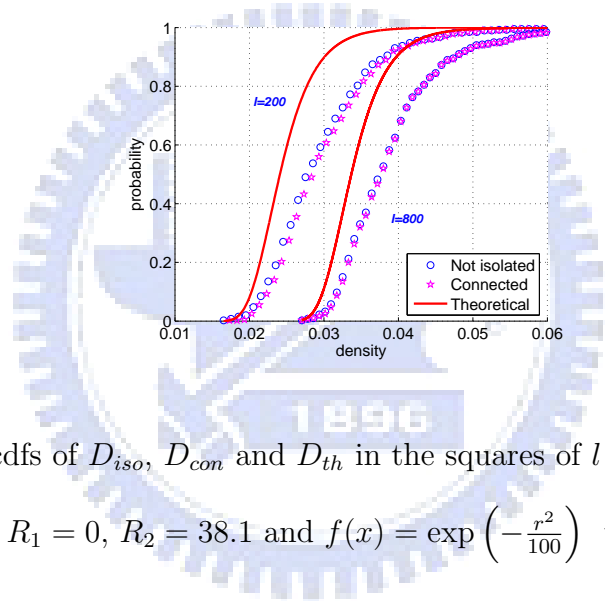


Figure 5.18: The cdfs of D_{iso} , D_{con} and D_{th} in the squares of $l = 200$ and $l = 800$ in fast fading model with $R_1 = 0$, $R_2 = 38.1$ and $f(x) = \exp\left(-\frac{r^2}{100}\right)$ without torus.

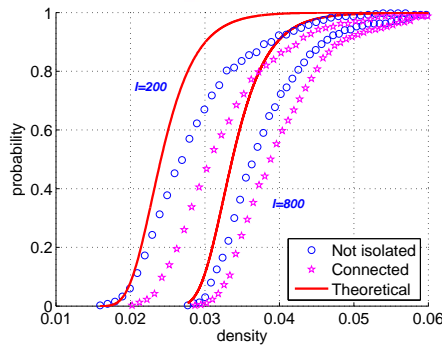


Figure 5.19: The cdfs of D_{iso} , D_{con} and D_{th} in the squares of $l = 200$ and $l = 800$ in Disk model with $R_1 = 0$, $R_2 = 10$ and $f(x) = 1$ without torus.

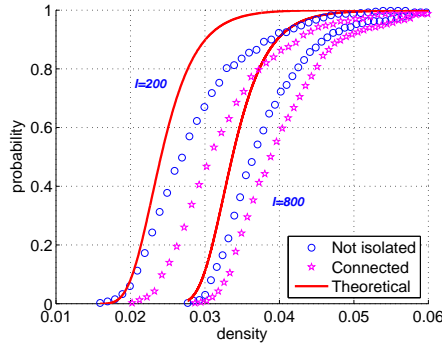


Figure 5.20: The cdfs of D_{iso} , D_{con} and D_{th} in the squares of $l = 200$ and $l = 800$ in Slow fading model with $R_1 = 0$, $R_2 = 13.18597$ and $f(x) = \frac{1}{2} \left(1 + \operatorname{erf} \left(\frac{5-5 \log r}{2\sqrt{2}} \right) \right)$ without torus.

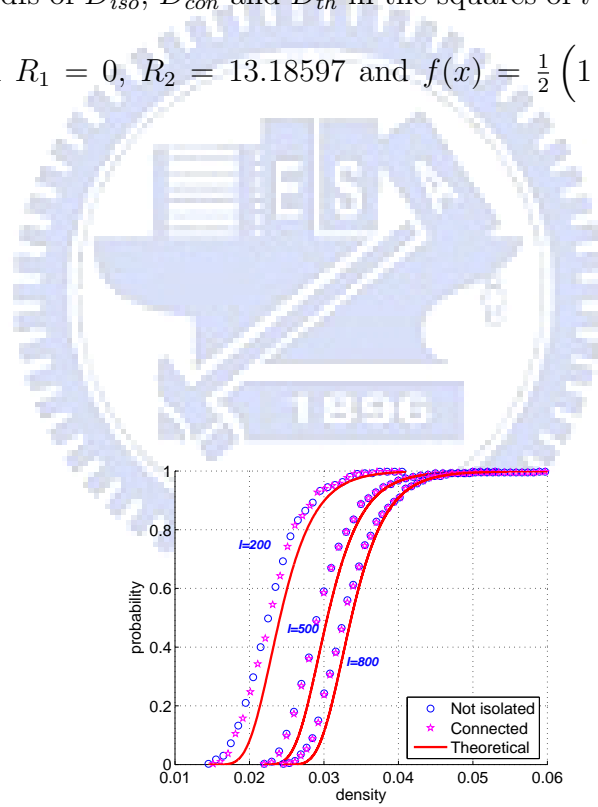


Figure 5.21: The cdfs of D_{iso} , D_{con} and D_{th} in the squares of $l = 200$ and $l = 800$ in fast fading model with $R_1 = 0$, $R_2 = 38.1$ and $f(x) = \exp \left(-\frac{r^2}{100} \right)$ without R2.

Chapter 6

Conclusions

In this work, we assume that the distribution of wireless nodes is modeled by a Poisson point process with mean density over a deployment region instead of a uniform deployment. Also, a generalized link model is proposed. By deploying nodes with adequate mean density, we can get the expected number of isolated nodes and the distribution of the number of isolated nodes. Theoretical derivation and simulations are elaborately demonstrated. In conclusion, the expected number of isolated nodes is $e^{-\omega}$ with certain constant ω and the distribution of the number of isolated nodes is asymptotically Poisson with mean $e^{-\omega}$. This information can help developer to design a wireless ad hoc and sensor network or to make decisions based on the demand of performance. Hopefully, the future research hopefully can loosen the restrictions on the deployment method and the deployment region.

Bibliography

- [1] O. Dousse, P. Thiran, and M. Hasler, “Connectivity in ad-hoc and hybrid networks,” in *Proceedings of the 21st Annual Joint Conference of the IEEE Computer and Communications Societies (INFOCOM 2002)*, vol. 2, 2002, pp. 1079–1088.
- [2] O. Dousse and P. Thiran, “Connectivity vs capacity in dense ad hoc networks,” in *Proceedings of the 23rd Annual Joint Conference of the IEEE Computer and Communications Societies (INFOCOM 2004)*, vol. 1, March 2004, pp. 476–486.
- [3] G. Zhang, J. Li, Y. Chen, and J. Liu, “Effect of mobility on the critical transmitting range for connectivity in wireless ad hoc networks,” in *Proceedings of the 19th International Conference on Advanced Information Networking and Applications (AINA 2005)*, vol. 2, March 2005, pp. 9–12.
- [4] X. Liu, “Coverage with connectivity in wireless sensor networks,” in *Proceedings of the 3rd International Conference on Broadband Communications, Networks and Systems (BROADNETS 2006)*, October 2006, pp. 1–8.
- [5] E. N. Gilbert, “Random plane networks,” *Journal of the Society for Industrial and Applied Mathematics*, vol. 9, no. 4, pp. 533–543, 1961.

- [6] H. Dette and N. Henze, “The limit distribution of the largest nearest-neighbour link in the unit d -cube,” *Journal of Applied Probability*, vol. 26, no. 1, pp. 67–80, 1989. [Online]. Available: <http://www.jstor.org/stable/3214317>
- [7] P. Gupta and P. R. Kumar, “Critical power for asymptotic connectivity in wireless networks,” in *Stochastic Analysis, Control, Optimization and Applications: A Volume in Honor of W. H. Fleming*, W. M. McEneaney, G. Yin, and Q. Zhang, Eds. Birkhauser, March 1998, pp. 547–566.
- [8] C.-W. Yi, P.-J. Wan, K.-W. Lin, and C.-H. Huang, “Asymptotic distribution of the number of isolated nodes in wireless ad hoc networks with unreliable nodes and links,” in *Proceedings of the Global Telecommunications Conference (IEEE GLOBECOM 2006)*, November 2006, pp. 1–5.
- [9] M. Haenggi, “Link modeling with joint fading and distance uncertainty,” in *Proceedings of the 4th International Symposium on Modeling and Optimization in Mobile, Ad Hoc and Wireless Networks*, April 2006, pp. 1–6.
- [10] S. Mukherjee and D. Avidor, “Connectivity and transmit energy considerations between any pair of nodes in a wireless ad hoc network subject to fading,” *IEEE Transactions on Vehicular Technology*, vol. 57, no. 2, pp. 1226–1242, March 2008.
- [11] R. Zhang and J.-M. Gorce, “Connectivity of wireless sensor networks with unreliable links,” in *Proceedings of the Second International Conference on Communications and Networking in China (CHINACOM 2007)*, August 2007, pp. 866–870.

- [12] P. Hall, *Introduction to the Theory of Coverage Processes*. New York, USA: John Wiley & Sons Inc, October 1988.
- [13] M. D. Penrose, “The longest edge of the random minimal spanning tree,” *The Annals of Applied Probability*, vol. 7, no. 2, pp. 340–361, 1997. [Online]. Available: <http://www.jstor.org/stable/2245234>
- [14] H. Zhang and J. Hou, “On deriving the upper bound of α -lifetime for large sensor networks,” in *Proceedings of the 5th ACM international symposium on Mobile ad hoc networking and computing (MobiHoc 2004)*. New York, NY, USA: ACM, 2004, pp. 121–132.
- [15] D. A. Griffith, *Advanced Spatial Statistics*. Dordrecht, The Netherlands: Kluwer Academic Publishers, April 1988.
- [16] C. Bettstetter, “On the minimum node degree and connectivity of a wireless multihop network,” in *Proceedings of the 3rd ACM international symposium on Mobile ad hoc networking & computing (MobiHoc 2002)*. New York, NY, USA: ACM, 2002, pp. 80–91.
- [17] T. S. Rappaport, *Wireless Communications: Principles and Practice*, 2nd ed. Prentice Hall PTR, January 2002.
- [18] A. F. Molisch, *Wireless Communications*. Wiley-IEEE Press, November 2005.
- [19] C. Bettstetter and C. Hartmann, “Connectivity of wireless multihop networks in a shadow fading environment,” *Wireless Networks*, vol. 11, no. 5, pp. 571–579, 2005.

- [20] M. Penrose, *Random Geometric Graphs*. New York, USA: Oxford University Press, July 2003.
- [21] P.-J. Wan and C.-W. Yi, “On the longest edge of gabriel graphs in wireless ad hoc networks,” *IEEE Transactions on Parallel and Distributed Systems*, vol. 18, no. 1, pp. 111–125, January 2007.

